Russian Chemical Reviews **73** (8) 753 – 770 (2004) © 2004 Russian Academy of Sciences and Turpion Ltd

DOI 10.1070/RC2004v073n08ABEH000898

Phosphate tungsten bronzes

V V Skopenko, V V Lisnyak, N V Stus, N S Slobodyanik

Contents

I.	Introduction	753
II.	Methods of synthesis	753
III.	Crystal structure	757
IV.	Electronic structure	764
V.	Electrophysical properties	766
VI.	Conclusion	767

Abstract. Theoretical and experimental data on the synthesis, structure, properties and applications of phosphate tungsten bronzes accumulated to date are systematised. Attention is focussed on interrelations between structural features and electrophysical properties of these compounds. Prospects for practical applications of phosphate tungsten bronzes are discussed. The bibliography includes 138 references.

I. Introduction

Recently, interest in macroscopic quantum phenomena such as superconductivity and laser effect has grown rapidly. Research into and application of these phenomena introduces fundamental concepts of quantum mechanics into everyday life.[1,2] Intensive studies of oxide bronzes (low-dimensional metallic conductors) have been carried out in the last ten to fifteen years. This is, in particular, due to the fact that these compounds possess macroscopic quantum properties, *e.g.*, electronic instabilities responsible for initiation of spin density waves (SDW) and charge density waves (CDW).[3–8]

The term 'oxide bronzes' was introduced by Friedrich Wohler in 1824 to name a series of oxide compounds of tungsten. Currently, the term is used for crystalline compounds of general formula M_xEO_n, where M is usually an alkali metal and E is a transition metal. Characteristic of the oxide bronzes are intense colour and metallic luster. These compounds can possess metallic or semiconducting properties. Usually, bronzes retain the structure of the starting oxide EO_2 or EO_3 when the element E can be in an oxidation state of less than 4 or less than 6, respectively, and are characterised by certain homogeneity regions.[9] Electrons of the dopant cations inserted into the starting oxide can be delocalised over the entire structure, thus being responsible for the onset of metallic-type conductivity. The semiconducting properties are due to the interaction of polyvalent metal ions through bridging oxygen atoms.

Oxide bronzes can exhibit high anisotropy (low dimensionality) of electronic conductivity owing to peculiarities of their crystal and electronic structures. For quasi-one-dimensional compounds the conductivity along a particular crystallographic direction is several orders of magnitude higher than along two other directions while for quasi-two-dimensional compounds the conductivities along two particular crystallographic directions are several orders of magnitude higher than the conductivity along the third direction. The crystal structures of the oxide bronzes represent three-dimensional frameworks; because of this, the dimensionality of electronic conductivity can be lower than the dimensionality determined from crystallographic data.

Many transition metal oxides (among them, superconducting copper oxides are best known) possess low-dimensional properties. This also holds for both molybdenum and tungsten oxide bronzes which undergo transitions to the CDW state.[10,11] Minor variations of thermodynamic parameters (temperature, pressure, chemical potential, *etc.*) can cause significant changes in the physical properties of compounds. Because of this 'thermodynamic susceptibility' these inorganic materials can serve as model objects in studies of various instabilities.

The available models for mechanisms of the onset of CDW are inadequate. Therefore, systematic studies are carried out of CDW in compounds which exhibit low-dimensional electrophysical properties but have different compositions and structures. Among the widely used model objects are the phosphate tungsten bronzes containing perovskite-type layers built of ReO_3-type corner-sharing WO_6 octahedra separated by layers comprised of monophosphate groups or diphosphate units. Redistribution of the electron density between the phosphate groups and the layers of WO_6 octahedra in the phosphate tungsten bronzes gives rise to a partially filled conduction band composed of hybridised p- and d-AOs. These structural features are also responsible for the metallic conductivity of bronzes and for two kinds of electronic instabilities, namely, Peierls transitions leading to the CDW state [12–18] and the superconducting state instabilities.[18,19]

II. Methods of synthesis

At present, three main groups of the phosphate tungsten bronzes are known. These are the monophosphate tungsten bronzes (MPTBs) of general formula $A_x(PO_2)_4(WO_3)_{2m}$ with pentagonal (MPTBp) [20–23] or hexagonal (MPTBh) [24,25] structural channels and the diphosphate tungsten bronzes (DPTBs) of general for-

V V Skopenko, V V Lisnyak, N V Stus, N S Slobodyanik Department of Chemistry, Kyiv National Taras Shevchenko University, ul. Vladimirskaya 64, 01033 Kyiv, Ukraine. Fax (38-044) 239 32 20. Tel. (38-044) 220 86 91, (38-044) 239 32 20 (V V Skopenko). Tel. (38-067) 977 95 62. E-mail: lisnyak@chem.univ.kiev.ua (V V Lisnyak). Tel. (38-044) 239 33 14. E-mail: stus@chem.univ.kiev.ua (N V Stus). Tel. (38-044) 234 51 85 (N S Slobodyanik)

Received 14 January 2004
Uspekhi Khimii **73** (8) 814 – 832 (2004); translated by A M Raevskiy

mula $A_x(P_2O_4)_2(WO_3)_{2m}$ (A is a vacancy or a monovalent or divalent cation) with hexagonal channels (DPTBh).[26, 27] Studies on phase formation in the systems $P_2O_5-WO_3-W$ and $A_2O-P_2O_5-WO_3-W$ began in the 1980s in connection with the search for new functional materials for semiconductor electronics.[28–34]

It should be noted that the phosphate tungsten bronzes are prone to form the intergrowth phases. This trend becomes more pronounced as the parameter m increases. Therefore, the MPTBp compounds with $m > 14$, MPTBh compounds with $m > 7$ and DPTBs with $m > 10$ have not been synthesised as regular single crystals.

1. Synthesis of polycrystals

Polycrystalline powders and small single crystals of a number of the phosphate tungsten bronzes were first obtained by solid-state reactions starting from tungsten trioxide, acid ammonium orthophosphates of different degree of substitution and metallic tungsten taken in the stoichiometric ratio. Here, choosing an optimum regime of synthesis of compounds of specified compositions is a challenge. Usually, the interaction of reagents involves two stages, (1) melting of tungsten trioxide with ammonium orthophosphate monohydrate in the temperature range 573–890 K for 24–48 h[20, 22, 24, 27] to form some intermediate ammonium-containing compounds and low-melting glasses[35] and (2) interaction of the product obtained with fine-grained tungsten powder at temperatures 1000–1473 K in inert atmosphere (evacuated ampoules) over a period of several weeks. In most cases the starting components are taken in a ratio that provides the desired stoichiometry of the reaction product. This technique permits the synthesis of powders and small crystals of good quality, which are often used for growth of single crystals.[36, 37]

Reduction by transition metals (in particular, tungsten) in multicomponent oxide systems is a nonequilibrium process. This leads to coexistence of the regions suitable for crystallisation of individual compounds and broad heterogeneous-heterophase regions in which co-crystallisation of several phases occurs in narrow temperature and concentration ranges.[25, 38, 39] The compositions of the compounds formed in multicomponent oxide systems strongly depend on the synthesis conditions, *i.e.*, the ratio of the starting reagents, their dispersion, temperature, presence of temperature gradients, duration of the reaction and on the presence of modifiers.

Unfortunately, no optimised general methods of preparation of polycrystalline phosphate tungsten bronzes are available as yet. It should be noticed that often crystallisation of compounds differing in composition and structure occurs under identical experimental conditions.

2. Growth of single crystals

One of the most widely used methods of growth of single crystals of the phosphate tungsten bronzes involves the use of various transport reactions (in the presence of temperature gradients) in the temperature range from 850 to 1473 K. Using this technique, it is possible to grow high-quality single crystals with typical dimensions $(1-3)\times(0.6-3)\times(0.1-0.75)$ mm over a period of one to three weeks.[40, 41] Here, the role of the transporting agents can be played by iodine, phosphorus pentaoxide and by the ammonium and some alkali metal iodides, bromides or chlorides. The method was optimised to obtain the following members of the MPTBp family: $(PO_2)_4(WO_3)_4$, $(PO_2)_4(WO_3)_8$ and $(PO_2)_4(WO_3)_{12}$.[42–44]

The possibility of control of chemical transport reactions using methods of chemical thermodynamics[45] (in particular, using the CVTRANS program package[46]) make this single-crystal growth technique attractive for both laboratory and large-scale applications.

Flux growth of crystals of phosphate tungsten bronzes using low-melting phosphate–tungsten and phosphate–tungstate–molybdate systems[38] and complex fluxes containing a glass-forming component (*e.g.*, SiO_2 and GeO_2[21, 38, 47, 48]) was found to be less promising owing to uncontrollable inclusion of impurities that deteriorate the electrophysical properties of materials.

At present, there are many methods of synthesis of polycrystals and single crystals of MPTBp compounds which crystallise in the form of plane-parallel plates with high reflectivity. Tables 1 and 2 list the synthesis conditions and characteristics of a number of MPTBp crystals.[49–55]

Table 1. Synthesis conditions and characteristics of $(PO_2)_4(WO_3)_{2m}$ crystals with $m = 2$ and 4.

m	Starting components	Synthesis conditions	Crystal colour, habit, size /mm	Ref.
Conditions for solid-phase synthesis of polycrystals				
2	$WOP_2O_7 + W$ (1 : 2)	1573 K	blue plates	49
4	$(NH_4)_2HPO_4 + WO_3 + W$ (see [a])	873 K, 1223 K (48 h), 1273 K	purple plates	50, 51
4	$(NH_4)_2HPO_4 + WO_3 + W$ (see [a])	1173 K, 1250 K	red plates	22
Conditions for synthesis of single crystals				
2	$P_2O_5 + W + WO_3$ (see [a])	heating of furnace from 873 to 1473 (1523) K for 6 h, storage for four days	dark brown plates, $2\times0.75\times0.2$	52
2	$P + WO_3$ (see [a, b])	1273–1173 K	maroon	43
2	$P_2O_5 + W + WO_3 + SiO_2$ (5 : 3 : 3 : 2)	1523 K (two or three days), 1373 K	maroon plates, $0.12\times0.09\times0.05$	21, 38
4	$(NH_4)_2HPO_4 + WO_3 + W$ (see [a])	heating from 873 to 1273 K at a rate of 200 K h^{-1}, two-zone furnace 1473/1273 K (a week), cooling down to 298 K	purple plates, $3\times3\times0.2$	50, 51
4	$(NH_4)_2HPO_4 + WO_3 + Tl_2CO_3 +$ + W (see [c])	573 (24 h), two-zone furnace, 1343 K (hot zone), $\Delta T = 130$ K (see [d])	purple plates, $1.5\times0.6\times0.3$	52

Note. Here and in Tables 2, 3 in the column 'Synthesis conditions' we present the parameters of the heat treatment regimes, *viz.*, temperatures and durations of corresponding stages (in parentheses). At the first temperature (often, the time of stay at this temperature is not reported in the original studies), the mixtures of the metal trioxide and metal phosphate (in some cases) and metal carbonate (in other cases) were initially heated. At the second temperature, metallic tungsten was added and the system was kept until complete interaction between the metal and other components. At the third temperature, particular bronzes were synthesised (cooling is accompanied by bronze crystallisation).

[a] The starting reagent ratio was calculated with respect to the stoichiometry of the reaction product. [b] Obtained with 0.5 mol.% I_2 as transporting agent. [c] Calculated with respect to the stoichiometry of the compound $TlP_4W_4O_{20}$; obtained with 5 mol.% KI as transporting agent. [d] ΔT is the temperature difference between the hot and cold zones.

Table 2. Synthesis conditions and characteristics of $(PO_2)_4(WO_3)_{2m}$ crystals with $m > 4$.

m	Starting components	Synthesis conditions	Crystal colour, habit, size /mm	Ref.
Conditions for solid-phase synthesis of polycrystals				
5	$(NH_4)_2HPO_4 + WO_3 + W$ (calculated with respect to the stoichiometry of the compound $P_4W_8O_{32}$)	873 K, 1223 K (48 h), 1273 K, cooling down to 300 K	blue-purple	50
5 4 + 6	$(NH_4)_2HPO_4 + WO_3 + W$ (calculated with respect to the stoichiometry of the compound $P_4W_{10}O_{38}$)	673 K, 1373 K (seven days)	dark blue 0.006 mm thick	53, 54
6	$(NH_4)_2HPO_4 + WO_3 + W$ (see [a])	873 K, 1173 K (few days)	prismatic	20
6	$(NH_4)_2HPO_4 + WO_3 + W$ (see [a])	923 K, 1273 K (four days), cooling at a rate 0.6 K h^{-1} down to 500 K	dark blue plates, $5.26 \times 3.1 \times 1.42$	38
7	$(NH_4)_2HPO_4 + WO_3 + W$ (calculated with respect to the stoichiometry of the compound $P_4W_{14}O_{50}$)	873 K (10 h), heating with a 100 K increment, two-zone furnace, 1473/1273 K (a week), cooling down to 600 K	dark blue plates	28
8	$(NH_4)_2HPO_4 + WO_3 + W$ (see [a])	873 K, 1173 K (few days)	purple-red plates	20
10	$(NH_4)_2HPO_4 + WO_3 + W$ (see [a])	873 K (12 h), 1273 K (48 h)	black plates, $1.5 \times 0.5 \times 0.3$	55
12	$(NH_4)_2HPO_4 + WO_3 + W$ (see [a])	873 K (12 h), 1273 K (48 h)	blue plates, $0.125 \times 0.07 \times 0.003$	51
Conditions for synthesis of single crystals				
5	$(PO_2)_4(WO_3)_8$ (see [b])	heating from 873 to 1273 K at a rate of 200 K h^{-1}, two-zone furnace, 1473/1273 K (a week), cooling down to 298 K	blue-purple plates with golden edges, $3 \times 3 \times 0.2$	50
7	$(PO_2)_4(WO_3)_{12}$ (see [b])	873 K (10 h), 873 K, two-zone furnace, 1473/1273 K (a week), cooling down to 600 K	purple plates, $0.69 \times 0.15 \times 0.075$	54
10	$(PO_2)_4(WO_3)_{20}$ (see [b])	two-zone furnace, 1473/1273 K (two weeks), $\nabla T = 10$ K cm^{-1} (see [c]), cooling down to 600 K	black plates, $1.5 \times 0.5 \times 0.3$	55
12	$(PO_2)_4(WO_3)_{24}$ (see [b])	two-zone furnace, 1473/1273 K (two weeks), $\nabla T = 10$ K cm^{-1} (see [c])	blue plates, $0.125 \times 0.07 \times 0.003$	51

[a] The ratio of the starting reagents was calculated with respect to the stoichiometry of the reaction product. [b] Recrystallisation from a mixture of compounds obtained by solid-phase synthesis. [c] ∇T is the temperature gradient.

3. Peculiar features of the synthesis of compounds $A_x(PO_2)_4(WO_3)_{2m}$ and $A_x(P_2O_4)_2(WO_3)_{2m}$

One of the most widely used methods of synthesis of compounds of the families $A_x(P_2O_4)_2(WO_3)_{2m}$ and $A_x(PO_2)_4(WO_3)_{2m}$ (Tables 3 and 4) is melting of stoichiometric mixtures of ammonium orthophosphates and tungsten trioxide (if A is a vacancy) and metal carbonates (if A is a monovalent or divalent metal) followed by interaction of the glass obtained with metallic tungsten in inert atmosphere.

The use of the flux technique to obtain these compounds has some peculiar features because the glass formation region is limited and the reaction is carried out at the liquid–metal interface. It should be noted that high reactivity of melts towards the crucible materials at $1153 \leqslant T \leqslant 1270$ K causes enrichment of the system with silicates or aluminates. Therefore, the synthesis of pure phases and studies on phase formation in the systems in question become much more complicated. The phase diagrams of pseudoquaternary systems were constructed only for a few isothermal sections in narrow concentration ranges, *viz.*, $KWO_3-WO_3-PWO_5$,[25] $Li_xWO_3-WO_3-PWO_5$,[38] $Na_xWO_3-WO_3-PWO_5$,[38] $K_4P_8W_4O_{32}-P_8W_4O_{32}-Na_4P_8W_4O_{32}$ and $K_4P_4W_{12}O_{44}-P_4W_{12}O_{44}-Na_4P_4W_{12}O_{44}$.[40, 68] The phase diagrams of the two last-mentioned systems exhibit broad multiphase regions, which casts some doubt upon their correctness.

In addition to the classical method of synthesis (see above) there is a variety of methods based on the chemical or electrochemical intercalation of cations into the MPTBp or MPTB frameworks containing cations in the structural channels. A number of sodium- and lithium-containing derivatives were obtained using the redox reactions with such organometallic reducing agents as LiC_4H_9 and $NaC_{10}H_8$.[28] In this case filling of the perovskite-type cavities in the bronze structure by cations occurs in contrast to the high-temperature methods of synthesis. Using the simplest electrochemical cells, $(+)|A|AClO_4Y|[(PO_2)_4(WO_3)_{2m}/A_x(PO_2)_4(WO_3)_{2m}]|(-)$ (A = Li, Na; Y = propylene carbonate), it is possible to control the synthesis of materials with different degrees of filling of structural channels with cations and to perform ion exchange by simple charge–discharge cycles.[28] Intercalation of cations to obtain compounds of the $A_x(P_2O_4)_2(WO_3)_{2m}$ family can also be achieved *via* chemical vapour transport reactions. For instance, the $A_x(PO_2)_4(WO_3)_8$ crystals were synthesised by reactions of the Group Ia element or Tl(I) iodides with $(PO_2)_4(WO_3)_{2m}$.[69]

4. Peculiarities of phase formation in the systems containing inserted polyvalent metal cations

Recently, numerous studies aimed at obtaining phosphate tungsten bronzes modified by homovalent and heterovalent substitution have been carried out. The compositions and crystallographic parameters of a number of compounds obtained are listed in Table 5.

At present, the absence of the phosphate molybdenum bronzes similar in structure and properties to the phosphate tungsten bronzes is a paradox with no explanation, though mixed molybdenum–phosphate bronzes are known.

The use of molybdenum as the reducing agent in mixed nitrate–phosphate systems leads to formation of low-melting fluxes and to shift of the heat treatment regimes towards lower

Table 3. Synthesis conditions and characteristics of crystals $A_x(PO_2)_4(WO_3)_{2m}$ and $A_x(P_2O_4)_2(WO_3)_{2m}$ obtained by solid-phase synthesis [melting of the components $A_2CO_3 + (NH_4)_2HPO_4 + W + WO_3$ (A = Na, K, Rb, Cs) and $BaCO_3 + (NH_4)_2HPO_4 + W + WO_3$ taken in the stoichiometric ratios].

Composition	Starting components	Synthesis conditions	Crystal colour, habit, size /μm	Ref.
Conditions for solid-phase synthesis of polycrystals				
$Na_{1.4}(PO_2)_4(WO_3)_8$	$Na_2CO_3 + (NH_4)_2HPO_4 + W + WO_3$	773 K, 1173 K (three days)	light-brown with copper reflection needles, $30 \times 48 \times 456$	56
$Na_{2.2}(PO_2)_4(WO_3)_{12}$	$Na_2CO_3 + (NH_4)_2HPO_4 + W + WO_3$	773 K, 1173 K (three days)	purple needles, $48 \times 60 \times 380$	56
$Na_2(PO_2)_4(WO_3)_{2m}$ ($4 \leqslant m \leqslant 13$) and $Na_3(PO_2)_4(WO_3)_{14}$	$Na_2CO_3 + (NH_4)_2HPO_4 + W + WO_3$	873 K, 1273 K (few days)	–	57
$K_x(PO_2)_4(WO_3)_8$ ($0.75 \leqslant x \leqslant 2$)	$K_2CO_3 + (NH_4)_2HPO_4 + W + WO_3$	873 K (12 h), 1223 K (48 h), cooling down to 298 K	purple needles	58
$K_x(PO_2)_4(WO_3)_{12}$ ($1 \leqslant x \leqslant 2$)	$K_2CO_3 + (NH_4)_2HPO_4 + W + WO_3$	873 K (12 h), 1223 K (48 h), cooling down to 298 K	dark purple rods, $60 \times 30 \times 10$	41
$K_x(P_2O_4)_2(WO_3)_{20}$ ($x \leqslant 0.25$)	$K_2CO_3 + (NH_4)_2HPO_4 + W + WO_3$	1173 K, 1373 K (ten to fifteen days), cooling for two days down to 300 K	dark blue plates, $14 \times 90 \times 262$	59
$K(P_2O_4)_2(WO_3)_{2m}$ ($5 \leqslant m \leqslant 10$)	$K_2CO_3 + (NH_4)_2HPO_4 + W + WO_3$	873 K, 1373 K (fifteen days)	dark blue and black	6
$K_x(P_2O_4)_2(WO_3)_{2m}$ ($4 \leqslant m \leqslant 10$, $x = 2$) ($2 \leqslant m \leqslant 20$, $1.5 \leqslant x \leqslant 4$)	$K_2CO_3 + (NH_4)_2HPO_4 + W + WO_3$	823 K, 1173 – 1473 K (four to eight days)	the same	60
$Rb(P_2O_4)_2(WO_3)_{2m}$ ($4 \leqslant m \leqslant 10$)	$Rb_2CO_3 + (NH_4)_2HPO_4 + W + WO_3$	873 K, 1373 K (fifteen days)	"	60
$Rb_{1.6}(P_2O_4)_2(WO_3)_6$	$Rb_2CO_3 + (NH_4)_2HPO_4 + W + WO_3$	900 K, 1230 K (eight days)	needles, $10 \times 76 \times 144$	61
$Rb_{0.44}(P_2O_4)_2(WO_3)_{14}$	$Rb_2CO_3 + (NH_4)_2HPO_4 + W + WO_3$	900 K, 1270 K (a week)	plates, $120 \times 18 \times 96$	62
$Rb_x(P_2O_4)_2(WO_3)_{16}$ ($1.6 \leqslant x \leqslant 2$)	$Rb_2CO_3 + (NH_4)_2HPO_4 + W + WO_3$	1173 K	plates, $18 \times 75 \times 280$	48
$Cs(P_2O_4)_2(WO_3)_4$	$Cs_2CO_3 + (NH_4)_2HPO_4 + W + WO_3$	1173 K, 1230 K (15 h)	maroon needles, $28 \times 40 \times 144$	63
$Ba(P_2O_4)_2(WO_3)_{16}$	$BaCO_3 + (NH_4)_2HPO_4 + W + WO_3$	873 K, 1473 K (48 h)	plates, $120 \times 18 \times 96$	27
$Ba(P_2O_4)_2(WO_3)_{2m}$ ($m = 6-10$)	$BaCO_3 + (NH_4)_2HPO_4 + W + WO_3$	(1173 – 1473), (six to twenty-one days), cooling down to 300 K	–	64
Conditions for synthesis of single crystals				
$K_x(PO_2)_4(WO_3)_8$ ($0.75 \leqslant x \leqslant 2$)	$K_x(PO_2)_4(WO_3)_8$ ($0.75 \leqslant x \leqslant 2$)	two-zone furnace, 1473 K/1273 K (a week), cooling down to 298 K (see [a])	purple plates, $60 \times 30 \times 10$	58
$K_x(PO_2)_4(WO_3)_8$ ($0.86 \leqslant x \leqslant 1.94$)	$K_x(PO_2)_4(WO_3)_8$ ($0.86 \leqslant x \leqslant 1.94$)	two-zone furnace, 1473 K/1273 K, (a week), cooling down to 298 K (see [a])	copper-coloured needles, $100 \times 20 \times 4$	8, 16
$K_x(PO_2)_4(WO_3)_{12}$	$K_x(PO_2)_4(WO_3)_{12}$	two-zone furnace, 1473 K/1273 K (a week), cooling down to 298 K (see [a])	purple plates, $60 \times 30 \times 10$	41
$Cs(P_2O_4)_2(WO_3)_4$	$Cs_2CO_3 + (NH_4)_2HPO_4 + W + WO_3$	923 K (see [b]), 1223 K (two weeks), cooling at a rate of 3 K h^{-1}	golden plates, $15 \times 20 \times 30$	65

[a] Stepwise cooling of the system (five steps of 200 K each). [b] Gas transport reaction with 5 mol.% KBr.

temperatures (673 – 873 K). It should be noted that the phase crystallisation processes in the $A_2CO_3 - H(NH_4)_2PO_4 - WO_3(MoO_3)$ systems and the structure of the resulting are strongly dependent on the composition, structure and physicochemical features (namely, differences between the thermochemical properties of the starting oxides and the melts formed, the type of short-range order in melts and the size of clusters comprised of the MO_6 octahedra) of the glasses formed in these systems.[71–77] Usually, the use of complex systems leads to the formation of compounds with mixed frameworks that differ from the frameworks of the phosphate tungsten bronzes.[70–77]

For instance, a $Na_{1+x}(Mo_{0.15}W_{1.85})O_5(PO_4)$ phase was crystallised in the system $Na_2CO_3 - H(NH_4)_2PO_4 - WO_3 - Mo$ in the temperature interval 673 – 903 K.[74] The framework of this phase is comprised of infinite ribbons analogous to those observed in the monophosphate tungsten bronzes $(PO_2)_4(WO_3)_8$ (see Ref. 50) and

Table 4. Existence regions of the compounds $A_x(PO_2)_4(MO_3)_{2m}$ and $A_x(P_2O_4)_2(MO_3)_{2m}$ (A is a monovalent or divalent cation or a vacancy; M = W, Mo).

System	Composition	Ref.
$MoO_3-(NH_4)_2HPO_4-WO_3-W$	$(PO_4)_2(W_{1-x}Mo_xO_3)_6$ ($0 \leqslant x < 0.26$),	66
$Li_2CO_3-(NH_4)_2HPO_4-WO_3-W$	$Li_x(P_2O_4)_2(WO_3)_6$ ($x \leqslant 0.167$),	66
$Na_2CO_3-(NH_4)_2HPO_4-WO_3-W$	$Na_2(PO_2)_4(WO_3)_{2m}$ ($4 \leqslant m \leqslant 10$), $Na_3(PO_2)_4(WO_3)_{14}$, $Na_2(PO_2)_4(WO_3)_{2m}$ ($m \leqslant 13$)	27, 56, 57
	$Na_x(PO_2)_4(WO_3)_{2m}$ ($2 \leqslant m \leqslant 20$; $1.1 \leqslant x \leqslant 4$, $m = 4$); $Na_x(PO_2)_4(WO_3)_{12}$ ($1.1 \leqslant x \leqslant 4$), pure phases $Na_x(PO_2)_4(WO_3)_{2m}$ ($m \leqslant 13$, $m \neq 5$)	57
	$Na_x(P_2O_4)_2(WO_3)_6$ ($x \leqslant 0.22$)	66
	$Na_x(PO_2)_4(WO_3)_8$ ($1.1 \leqslant x \leqslant 1.5$, 2), $Na_x(PO_2)_4(WO_3)_{12}$ ($1.6 \leqslant x \leqslant 4$),	57
$K_2CO_3-(NH_4)_2HPO_4-WO_3-W$	$K_x(P_2O_4)_2(WO_3)_{20}$ ($x \leqslant 0.25$)	26
	$K(P_2O_4)_2(WO_3)_{2m}$ ($5 \leqslant m \leqslant 10$)	60
	$K_2(P_2O_4)_2(WO_3)_{2m}$ ($2 \leqslant m \leqslant 20$); $K_x(P_2O_4)_2(WO_3)_{2m}$ ($x > 1$, MPTBh; $x \leqslant 1$, DPTBh); compounds formed in the system K–W–P–O are as follows: MPTBp ($x = 0$), DPTBp ($x = 1$), MPTBh ($x = 2$); $1.75 \leqslant x \leqslant 3$, $m = 4-10$, $m \neq 5$; mixtures of the compounds with $m = 9$ and 10; mixtures of the MPTBh compounds and K_xWO_3 ($x = 3$, $m \leqslant 10$); mixtures of the compounds WO_3, K_xWO_3 and DPTBh ($x = 3$, $m > 10$)	60
$Rb_2CO_3-(NH_4)_2HPO_4-WO_3-W$	$Rb(P_2O_4)_2(WO_3)_{2m}$ ($4 \leqslant m \leqslant 10$)	60
	$Rb_{1.6}(P_2O_4)_2(WO_3)_6$	61
	$Rb_{0.44}(P_2O_4)_2(WO_3)_{14}$	62
	$Rb_x(P_2O_4)_2(WO_3)_{16}$ ($1.6 \leqslant x \leqslant 2$)	48
$BaCO_3-(NH_4)_2HPO_4-WO_3-W$	$Ba_x(PO_2)_4(WO_3)_{2m}$ ($6 \leqslant m \leqslant 10$; $m = 11-17$)	27
	$Ba(P_2O_4)_2(WO_3)_{2m}$ ($m = 6-10$)	64
$Cs_2CO_3-(NH_4)_2HPO_4-WO_3-W$	$Cs(P_2O_4)_2(WO_3)_4$	63, 65
	$Cs_{1-x}(P_2O_4)_2(WO_3)_4$ ($0 \leqslant x \leqslant 0.46$)	67
$Cs_2CO_3-Rb_2CO_3-(NH_4)_2HPO_4-WO_3-W$	$Cs_xRb_y(P_2O_4)_2(WO_3)_4$ ($0.72 \leqslant x \leqslant 0.97$, $0.16 \leqslant y \leqslant 0.33$)	67
$Cs_2CO_3-Na_2CO_3-(NH_4)_2HPO_4-WO_3-W$	$Cs_{0.89}Na_{0.17}(P_2O_4)_2(WO_3)_4$	67
$Cs_2CO_3-MoO_3-(NH_4)_2HPO_4-WO_3-W$	$Cs(P_2O_4)_2(W_{1-x}MO_xO_3)_4$ ($0. \leqslant x \leqslant 0.26$)	67
$PbCO_3-(NH_4)_2HPO_4-WO_3-W$	$Pb_x(PO_2)_4(WO_3)_{2m}$ [$6 \leqslant m \leqslant 10$; $x = 0.66$ ($m = 7$)]	7

Table 5. Systems studied and crystallographic characteristics of the phases obtained.

System	Composition	Space group	Unit cell parameters [a]					Ref.
			a /Å	b /Å	c /Å	β /deg	Z	
$CsNO_3-(NH_4)_2HPO_4-WO_3-W-V_2O_5$	$Cs_5VW_4O_9VO_4(PO_4)_4$	$Cmc2_1$	14.948	20.008	9.942	–	4	70
$RbNO_3-(NH_4)_2HPO_4-WO_3-Mo-MoO_3$	$Rb_2Mo_2WO_5(PO_4)_3$	$P2_1/n$	10.756	9.493	15.478	108.99	4	71
$K_2CO_3-(NH_4)_2HPO_4-WO_3-Mo-MoO_3$	$K_{6.6}Mo_{2.36}W_{3.64}O_{15}(PO_4)_4$, $K_7Mo_{6-x}W_xP_4O_{31}$ ($2 \leqslant x \leqslant 4$)	$R\bar{3}$	17.545	15.714	–	–	6	72
$Na_2CO_3-(NH_4)_2HPO_4-WO_3-Mo-MoO_3$	$Na_{0.75}(Mo_{0.42}W_{0.58})(Mo_{0.75}W_{0.25})O_3(PO_4)_2$, $Na_xMo_{2-y}W_yP_2O_{11}$ ($0.25 \leqslant x \leqslant 1$, $1.75 \leqslant y \leqslant 0.25$)	$P2_1/m$	7.200	6.369	9.123	106.29	2	73
	$Na_{1.3}(Mo_{0.15}W_{0.15})(W_{1.7})O_5(PO_4)_2$, $Na_2Mo_yW_{2-y}PO_9$ ($0.15 \leqslant y \leqslant 0.75$)	$P2_12_12_1$	4.853	8.516	16.646	–	4	74
$Li_2CO_3-(NH_4)_2HPO_4-WO_3-Mo-MoO_3$	$LiMo_{0.68}W_{1.32}O_3(PO_4)_2$	$C2/m$	8.142	6.361	7.728	102.45	2	75
	$Li_{0.5}MoWO_3(PO_4)_2$	$P2_1/m$	7.735	12.655	8.324	105.97	4	76
	$(Mo_xW_{2-x})O_3(PO_4)_2$ ($0 \leqslant x \leqslant 1.25$)	$P2_1/m$	7.827	12.538	7.833	92.36	2	77

[a] Data of single-crystal X-ray diffraction studies.

$A_x(PO_2)_4(WO_3)_8$ (see Ref. 56) but the fashion in which the ribbons are connected by PO_4 tetrahedra and the shape of channels where the sodium atoms reside are different. One metal position in the MO_6 octahedra is occupied by tungsten atoms only while the other is occupied by the statistically disordered molybdenum and tungsten atoms.[74] The framework of the compound $K_{6.6}Mo_{2.36}W_{3.64}O_{15}(PO_4)_4$ is built of $[MO_5]_\infty$ (M = W, Mo) spiral chains with alternating *cis*- and *trans*-bonds M–O–M. The chains are connected through PO_4 tetrahedra.[72]

Most mixed molybdenum–tungsten phosphates contain isolated MO_6 octahedra or M_2O_{11} bioctahedra. These are, *e.g.*, compounds $Cs_5VW_4O_9VO_4(PO_4)_4$,[70] $Rb_2Mo_2WO_5(PO_4)_3$,[71] $Na_{0.75}(Mo_{0.42}W_{0.58})(Mo_{0.75}W_{0.25})O_3(PO_4)_2$ (Ref. 73) and $Li_{0.5}MoWO_3(PO_4)_2$.[75,76]

In contrast to molybdenum, niobium does form the niobium phosphate bronzes. This permits the synthesis of mixed bronzes $(Nb_{0.787}W_{0.213})_4O_4(PO_4)_4$ (see Ref. 78) and $K_{3.75}Nb_{8.5-x}.W_xO_{14}(PO_4)_4$.[79] At the same time, compounds of the family $A_x(NbW)_5O_9(PO_4)_3$ (A = Li, K, Rb and Cs)[80] obtained in the systems $A_2CO_3-H(NH_4)_2PO_4-WO_3-W-Nb_2O_5$ contain distorted perovskite-type layers in which some WO_6 octahedra are replaced by PO_4 tetrahedra.

III. Crystal structure

Unlike the oxide tungsten bronzes A_xWO_3 (A = Li, Na, K, Rb, Cs) (Fig. 1 *a–c*) containing three-dimensional frameworks built of WO_6 octahedra, two families of the phosphate tungsten

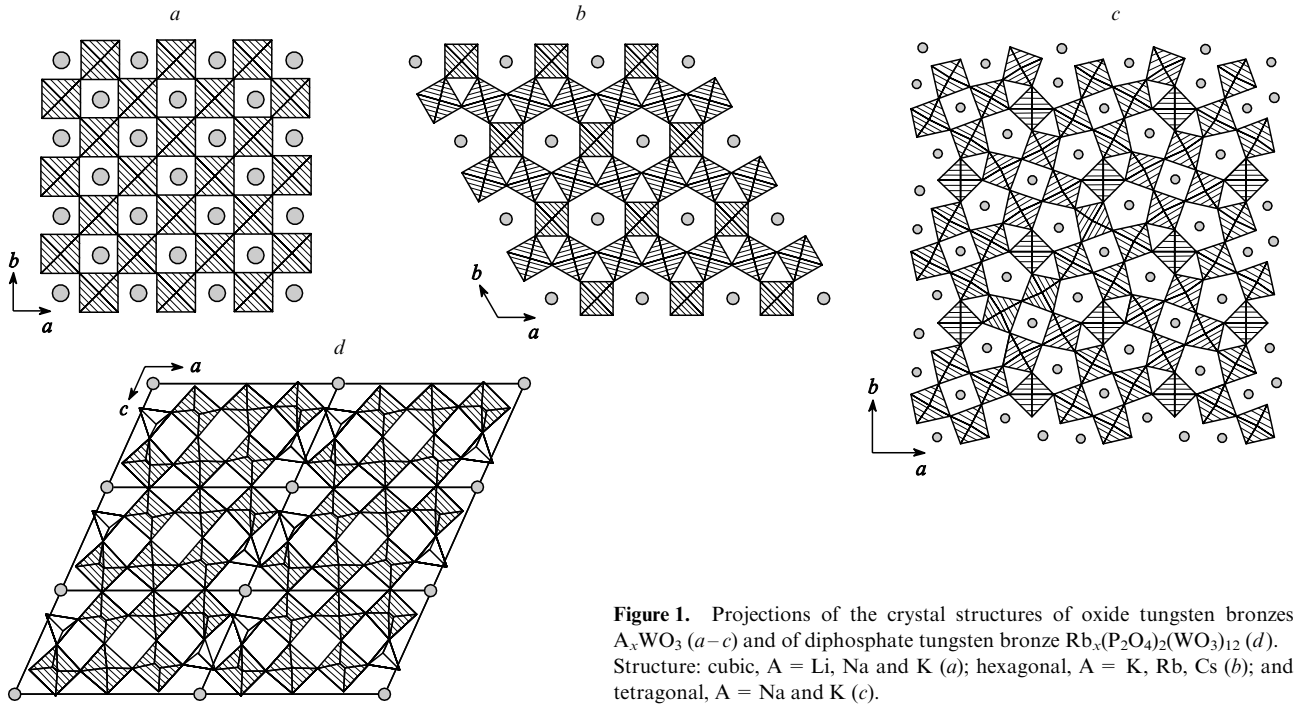


Figure 1. Projections of the crystal structures of oxide tungsten bronzes A_xWO_3 (*a*–*c*) and of diphosphate tungsten bronze $Rb_x(P_2O_4)_2(WO_3)_{12}$ (*d*). Structure: cubic, A = Li, Na and K (*a*); hexagonal, A = K, Rb, Cs (*b*); and tetragonal, A = Na and K (*c*).

bronzes, $A_x(PO_2)_4(WO_3)_{2m}$ and $A_x(P_2O_4)_2(WO_3)_{2m}$ (A is a vacancy or Na, K, Rb, Cs, Pb and Ba), contain chains or layers comprised of WO_6 octahedra connected by phosphate groups (see, *e.g.*, Fig. 1 *d*).

Because of (i) redistribution of the electron density in the mixed framework formed by the WO_6 octahedra and PO_4 tetrahedra and (ii) insertion of additional cations the oxidation state of the tungsten atoms in the phosphate tungsten bronzes usually varies between 5 and 6. Sharing of 4d electrons of the tungsten atoms and their delocalisation over the system of the W–O–W–O bonds lead to quasi-metallic electrophysical properties of the oxide and phosphate tungsten bronzes.[29,30]

The frameworks of the phosphate tungsten bronzes comprise corner-sharing WO_6 octahedra connected in the same manner as in the ReO_3-type cubic oxide tungsten bronzes (Fig. 2). In contrast to the oxide bronzes the perovskite-type blocks built of WO_6 octahedra in the frameworks of the phosphate tungsten bronzes are linked by PO_4 tetrahedra or by diphosphate units, P_2O_7. Depending on the value of the parameter *m*, these blocks can be chains (for the first members of each series with $m = 2$, see Fig. 3) or layers with the thickness increasing with *m*.

The frameworks of both the monophosphate and diphosphate tungsten bronzes containing perovskite-type layers are built based on similar principles. Namely, linear (DPTBs) or zigzag (MPTBs) slabs comprised of corner-sharing WO_6 octahedra are linked together to form infinite ribbons of composition W_mO_{4m+1} and W_mO_{4m+2}, respectively. The ribbons are connected in such a way

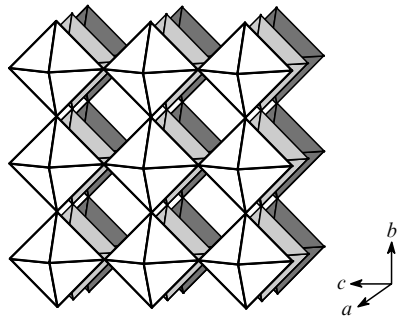


Figure 2. Structure of ReO_3.

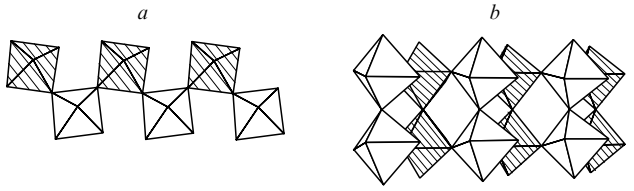


Figure 3. $(WO_5)_\infty$ chains in the structure of $(PO_2)_4(WO_3)_4$ (*a*) and $(WO_4)_\infty$ chains in the structure of $Rb_{0.5}(P_2O_4)_2(WO_3)_4$ (*b*).

that the first tungsten atom of each ribbon is bound to the third tungsten atom of the preceding ribbon through an axial oxygen atom. This results in the formation of perovskite-type layers containing corner-sharing octahedra only (the examples for $m = 4$ are shown in Fig. 4).

Usually, the layer thickness is expressed *via* the length of the linear chains of WO_6 octahedra and running along the directions of the perovskite crystallographic axes directed from the centre of an octahedron towards its vertices. The number of octahedra in two adjacent chains running along the $[001]_{per}$ axis (hereafter the subscript 'per' refers to the perovskite structure) is the same ($m/2$) for the even members of the series or differs by unity ($[(m+1)/2]$ and $[(m-1)/2]$) for the odd ones. The length of a chain of WO_6 octahedra along the $[010]_{per}$ and $[100]_{per}$ crystallographic directions equals *m* for any value of this parameter.

The orientation of the layer of octahedra can be determined with respect to the perovskite crystallographic axes; these layers are parallel to the $(112)_{per}$ plane in MPTBs and to the $(102)_{per}$ plane in DPTBs (see Fig. 4).

The phosphate or diphosphate groups are more strongly bound to one layer of WO_6 octahedra, namely, the PO_4 tetrahedra share three vertices with this layer, being connected to the adjacent layer through one vertice; while P_2O_7 units share four and two vertices, respectively. Therefore, the phosphate groups can be treated as constituents of the layer of octahedra. Different lengths of the bonds between adjacent oxygen atoms in WO_6 octahedra [$d(O-O) \approx 2.7$ Å] and in PO_4 tetrahedra [$d(O-O) \approx 2.5$ Å] lead to distortion of the octahedra linked to the phosphate groups. The structure distortion decreases on going towards the midpoint of the layer of octahedra. The inserted monovalent and divalent

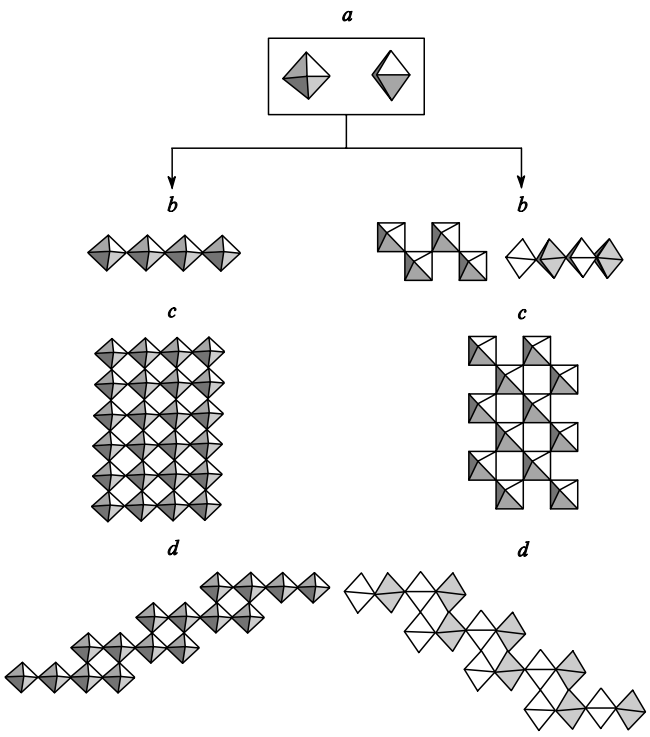


Figure 4. Structures of perovskite-type layers in the DPTB (on the left) and MPTB (on the right) compounds.
Isolated octahedra (*a*); W_4O_{21} blocks (*b*); W_4O_{17} units (on the left) and W_4O_{18} ribbons (on the right) (*c*); and the W_4O_{15} (on the left) and W_4O_{16} (on the right) layers (*d*) built of layers running normal to the plane of this Figure.

metal cations can be located within cavities of the framework which are connected by 'windows' of different shape and size.

Structural phase transitions in the phosphate tungsten bronzes can occur owing to the possibility of small tilts of octahedra in the perovskite-type layers and to ordering of the inserted cations within cavities of the framework.

1. Structural features of monophosphate tungsten bronzes

Two adjacent $W_mO_{4m}(PO_2)_2$ layers in the structure of the monophosphate tungsten bronzes $A_x(PO_2)_4(WO_3)_{2m}$ (A is a vacancy or Na, Ag, K, Pb) can be connected in two ways (see Fig. 5). In the first case, the layers are related by translation; all octahedra in the structure have the same orientation and cavities connected by hexagonal 'windows' are formed at the junction. In the second case, the layers are related by rotation about a twofold axis and cavities connected by pentagonal 'windows' are formed at the junction. Therefore, different (parallel or antiparallel) mutual orientations of layers lead to two families of the monophosphate tungsten bronzes with somewhat incorrect names, *viz*., the MPTBs with hexagonal and pentagonal channels (MPTBh and MPTBp, respectively). The frameworks of the monophosphate tungsten bronzes contain two types of cavities differing in shape and size. Cavities delimited by eighteen oxygen atoms (O_{18}) are surrounded by eight WO_6 octahedra and four PO_4 tetrahedra. The layer of octahedra contains perovskite-type cavities framed by twelve oxygen atoms (O_{12}) and connected by tetragonal 'windows'. All the structural data available at the moment indicate that monovalent or divalent cations be located only in the O_{18} cavities, whereas positions in the O_{12} cavities remain unoccupied.

Both MPTBp and MPTBh are structurally similar to the Magnéli phases containing perovskite-type layers built of MoO_6 octahedra isostructural to the W_4O_{16} layers of the monophosphate tungsten bronzes with $m = 4$. In γ-Mo_4O_{11} and η-Mo_4O_{11}, the layers built of octahedra are linked through MoO_4 tetrahedra similarly to the MPTBp and MPTBh, respectively.

Intercalation of lithium and sodium into different-type phosphate tungsten bronzes was first studied by Wang and Greenblatt [28] who reported the possibility of nearly complete filling of the perovskite cavities. However, these results require confirmation. Unfortunately, no structural studies of the bronzes obtained were performed.

The variety of symmetry types in the case of MPTB structures is due to small tilts of octahedra in the perovskite-type layer. In contrast to the WO_3 structure which permits tilting of the corner-sharing octahedra relative to three perovskite crystallographic axes, only tilting with respect to the $[001]_{per}$ direction is possible for the MPTBs. If the phosphate tungsten bronzes contain inserted cations, small tilts of octahedra in the perovskite-type

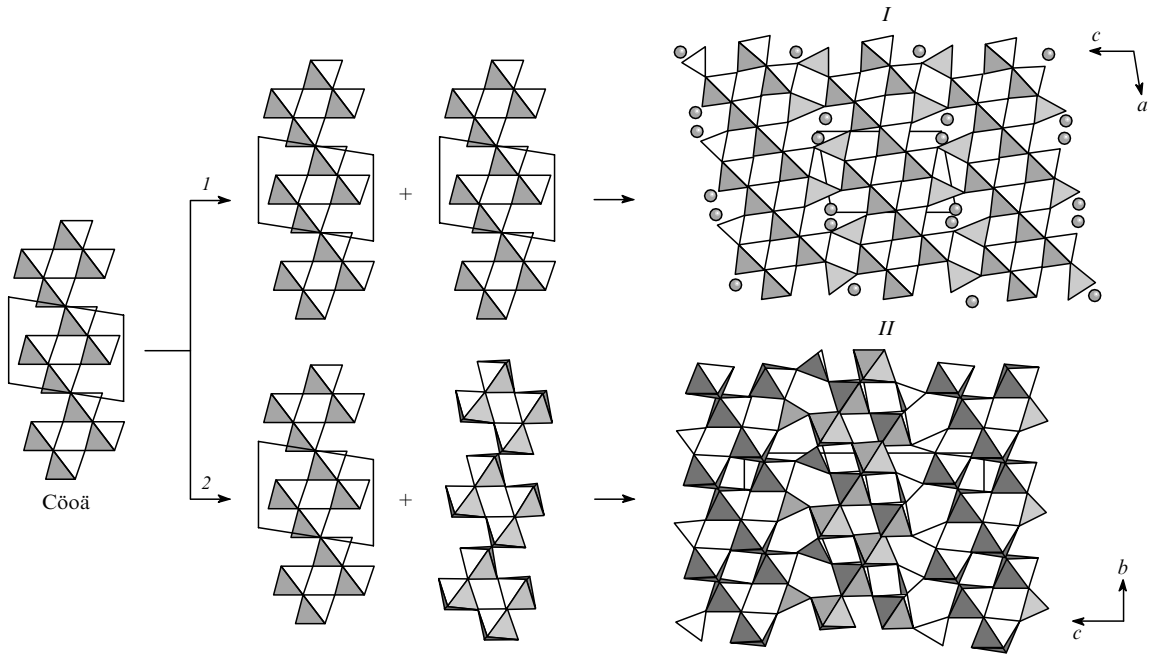


Figure 5. Parallel (*1*) and antiparallel (*2*) orientation of layers in the structures of the MPTBh (*I*) and MPTBp (*II*) compounds with $m = 4$.

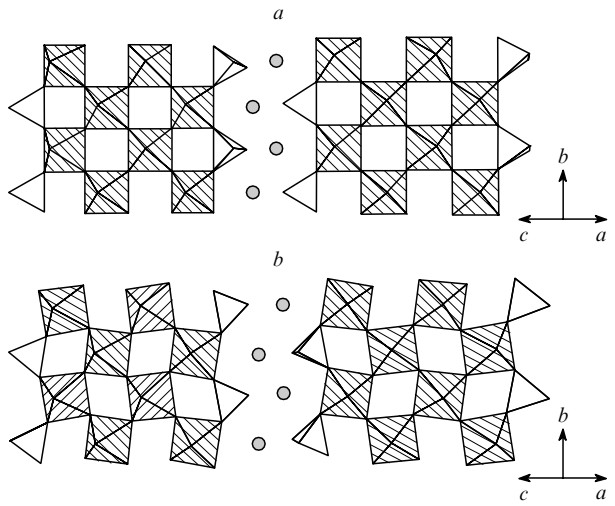


Figure 6. $(PO_2)_2(W_4O_{18})$ chains in the structures of $K_x(PO_2)_4(WO_3)_4$ (*a*) and $Na_x(PO_2)_4(WO_3)_4$ (*b*).

layer cause displacements of the cations located in the cavities and thus changes in the cavity shapes. Among the $A_x(PO_2)_4(WO_3)_{2m}$ bronzes (A = K, Na), small tilts by about 8.5° occur only in the sodium-containing compounds, whereas octahedra in the perovskite-type layer of the potassium-containing MPTBh are untilted (Fig. 6 *a*). In the $Na_x(PO_2)_4(WO_3)_{2m}$ bronze with $x < 4$ all octahedra in the linear chain running along the $[001]_{per}$ direction are rotated in one direction; correspondingly, octahedra in the four adjacent chains are rotated in the opposite direction (Fig. 6 *b*).

2. Monophosphate tungsten bronzes with pentagonal channels

Most of the MPTBp compounds have a general formula $(PO_2)_4(WO_3)_{2m}$. Structural features of this family of bronzes have been studied in most detail. The structure of the MPTBp with $m = 2$ contains the $(WO_5)_\infty$ chains instead of layers. In spite of this two tetrahedra and three octahedra also form pentagonal 'windows' similarly to other MPTBp compounds (Fig. 7). The unit cell parameters (in a standard setting) of the MPTBp compounds with the same thickness of the layer of octahedra are related to the perovskite unit cell parameters as follows:

$$a_{MPTBp} \approx a_{per}\sqrt{2},\ b_{MPTBp} \approx b_{per}\sqrt{3},$$

$$c_{MPTBp} \approx K + m a_{per}\cos 35^\circ \text{ (see Ref. 68)},$$

$$a_{MPTBp} \| [1\bar{1}0]a_{per},\ b_{MPTBp} \| [11\bar{1}]a_{per},\ c_{MPTBp} \| [112]a_{per}.$$

Here K is a constant related to the size of the PO_4 tetrahedron ($K \approx 2 \times 2.45$ Å) and 35° is the angle between the c_{MPTBp} axis and the $[001]_{per}$ axis. The unit cell thus defined has an orthorhombic symmetry with the a and b lattice constants being independent of m value. The c lattice constant linearly increases as m increases. The a_{MPTBp} and b_{MPTBp} parameters (~5.3 Å and ~6.55 Å, respectively) are close to the doubled face height and doubled edge length of the WO_6 octahedron, respectively.

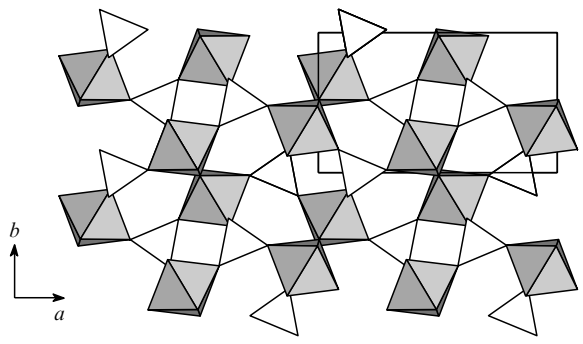


Figure 7. Projection of the crystal structure of $(PO_2)_4(WO_3)_4$.

In addition to the standard setting, a unit cell setting with the crystallographic axes running parallel to the perovskite axes is also used. If two layers of different thickness (m and m') alternate, the bronze unit cell becomes monoclinic with the following parameters [51]

$$d_{001} = K + 0.5(m + m')a_{per}\cos 35^\circ,$$

$$\tan \alpha_{MPTBp} = \frac{d_{001}}{0.5}(m - m')a_{per}\sin 35^\circ,$$

$$c_{MPTBp} = \frac{d_{001}}{\sin \alpha_{MPTBp}},$$

$$a_{MPTBp} = a_{per}\sqrt{2},$$

$$b_{MPTBp} = a_{per}\sqrt{3}.$$

Only one member of the MPTBp family (compound with $m = 5$) was obtained as two polymorphs. The structure of the first polymorph is characterised by regular alternation of the layers comprised of four and six octahedra, while the structure of the second polymorph is built of identical layers comprising five octahedra each. The structures of other MPTBp compounds contain layers of the same thickness, though irregular intergrowth of phases with different m occurs not infrequently [according to high-resolution transmission electron microscopy (HRTEM) data]. The probability of formation of the intergrowth phases increases as the m value increases.

The symmetry of many members of the MPTBp family is reduced with respect to an ideal structural type due to the possibility of small tilting of octahedra and to a different fashion of layer connection. Only one type of tilting is realised within the perovskite-type layer, the directions of tilting in two adjacent layers being the same or opposite. Taking into account different symmetry of the bronzes with the even and odd m values, the MPTBp compounds can crystallise in four structural types. The unit cell parameters of the MPTBp bronzes with the reliably (X-ray) established structures are listed in Table 6.

Most of the structures of MPTBp compounds studied by single-crystal X-ray diffraction analysis are characterised by symmetries lower than orthorhombic one. Studies of the MPTBp bronzes with large m values revealed satellite reflections indicating structure modulation at room temperature. The modulated structure of compound $(PO_2)_4(WO_3)_{20}$ with $m = 10$ was refined.[55] Structure modulation in the bronzes with small m values occurs only at low temperatures. For instance, a synchrotron radiation study of $(PO_2)_4(WO_3)_8$ (a compound with $m = 4$) at 20 K revealed structure modulation. All the MPTBp studied exhibited small tilting of octahedra, the tilt angle (8°) approaching that characteristic of WO_3.[89]

It has long been accepted that intercalation of cations into an MPTBp matrix is impossible and that crystallisation in the presence of inserted cations leads to the MPTBh compounds. The first members of the MPTBp families of composition $Na_x(PO_2)_4(WO_3)_{2m}$ with $0 \leqslant x \leqslant 1$ (isolated as individual compounds only for $m = 6$) were obtained only recently in the studies of phase relations in the systems $K_4(PO_2)_4(WO_3)_{2m}-Na_4(PO_2)_4.(WO_3)_{2m}-(PO_2)_4(WO_3)_{2m}$ with $m = 4$ and 6.[40] The $A_x(PO_2)_4.(WO_3)_{2m}$ bronzes were synthesised by intercalating monovalent cations (A = Li, Na, Ag, K) into the MPTBp structures.[90]

Changes in the structure of the MPTBp compound with $m \leqslant 14$ as a function of temperature have been reported in several studies (see, *e.g.*, Refs 2 and 15). A number of phase transitions related to periodic lattice distortions were detected at different

Table 6. Crystallographic parameters of the $(PO_2)_4(WO_3)_{2m}$ compounds with $m = 2-14$ obtained from single-crystal X-ray diffraction studies.

Composition	m	Space group	Unit cell parameters				Ref. [a]
			a /Å	b /Å	c /Å	angle /deg	
$P_4W_4O_{20}$	2	$P2_1cn$	5.231(3)	6.552(2)	11.117(1)	–	21, 54 (49, 38, 52)
$P_4W_8O_{32}$	4	$P2_12_12_1$	5.285(2)	6.569(1)	17.351(3)	–	50, 51 (15, 23, 38, 81–83)
$P_4W_{10}O_{38}$	5	$P2_1/n$	5.283(2)	6.574(39	20.451(1)	$\beta = 90.40(2)$	50 (23, 38, 84, 86)
$P_4W_{10}O_{38}$	6+4	$P2_1$	5.2850(2)	6.5656(2)	20.573(15)	$\alpha = 96.18(1)$	54 (23)
$P_4W_{12}O_{44}$	6	$P2_12_12_1$	5.2927(1)	6.5604(1)	23.549(3)	–	20 (15, 23, 82, 83, 87, 88)
$P_4W_{14}O_{50}$	7	$P2_1/n$	5.293(1)	6.571(3)	26.65(2)	$\beta = 90.19(1)$	54 (23, 82, 87, 88)
$P_4W_{16}O_{56}$	8	$P2_12_12_1$	5.2943(1)	6.5534(0)	29.700(4)	–	20 (2, 23, 85)
$P_4W_{18}O_{62}$	9	$P\bar{1}$	5.283(1)	6.571(3)	32.79(2)	$\alpha = 90.0(1)$, $\beta = 90.2(2)$, $\gamma = 89.78(1)$	81 (2, 20, 23, 83, 85)
$P_4W_{20}O_{68}$	10	$P2_1$	5.332(1)	6.551(2)	35.82(2)	$\beta = 90.6(2)$	55 (2, 38, 81, 83, 85)
$P_4W_{24}O_{80}$	12	$P2_12_12_1$	5.312(1)	6.5557(8)	42.196(8)	–	51 (81)
$P_4W_{28}O_{92}$	14	$P2_1/n$	5.321(1)	6.543(2)	48.00(5)	$\gamma = 91.04(2)$	81 (2, 38)

[a] Given in parentheses are the references to alternative solutions to the corresponding structures (including X-ray phase analysis data).

temperatures. These transitions correspond to anomalies of the temperature dependence of the electronic properties.

3. Monophosphate tungsten bronzes with hexagonal channels

The monophosphate tungsten bronzes with hexagonal channels have a general formula $A_x(PO_2)_4(WO_3)_{2m}$ (A = Na, Ag, K, Pb, Tl). In accord with the general framework build-up pattern, the unit cell symmetry cannot be higher than monoclinic one. Usually, the monoclinic cell is set in such a way that the twofold axis runs along the b direction. The unit cell parameters in the standard setting are as follows:[25]

$$a_{\mathrm{MPTBh}} \approx \sqrt{3}\, a_{\mathrm{per}}\,,\ b_{\mathrm{MPTBh}} \approx \sqrt{2}\, a_{\mathrm{per}}\,,$$

$$c_{\mathrm{MPTBh}} \sin\beta \approx 0.5\, K\ + 0.5\, m\, a_{\mathrm{per}} \cos 35^\circ,$$

$$a_{\mathrm{MPTBh}} || [11\bar{1}]_{\mathrm{per}}\,,\ b_{\mathrm{MPTBh}} || [1\bar{1}0] a_{\mathrm{per}}\,,\ c_{\mathrm{MPTBh}} || [112]_{\mathrm{per}}\,.$$

The parameters a_{MPTBh} and b_{MPTBh} are nearly 6.55 and 5.3 Å, respectively. Members of this series of bronzes with odd m values and most compounds containing sodium and lead are characterised by doubling of the c constant compared to the value calculated using the relation given above. The crystallographic parameters of MPTBh compounds obtained using data of X-ray studies are listed in Table 7.

The tilt angle of octahedra in the MPTBh bronzes depends on the size and content of inserted cations. For instance, all $Na_x(PO_2)_4(WO_3)_{2m}$ compounds with $x < 2$ are characterised by a tilt angle of nearly 8.5°. This angle decreases to 6.5° for the $Pb_x(PO_2)_4(WO_3)_{2m}$ bronzes with $6 \leqslant m \leqslant 10$. No tilt of octahedra was found in $Na_4(PO_2)_4(WO_3)_8$ and $K_x(PO_2)_4(WO_3)_{2m}$. These differences can be explained by the larger size of potassium ions and by the impossibility of redistribution of sodium cations in the cavities when all positions in $Na_4(PO_2)_4(WO_3)_8$ are occupied. At the same time each compound probably exists in two forms, a high-temperature form with non-tilted octahedra and a low-temperature form with tilted octahedra. At present, only the MPTBh compounds with alternation of the tilt direction from one layer to another are available. In the case of small tilts of octahedra the oxygen atom through which layers are linked virtually retains its position. This permits the formation of various intergrowth phases (layers with different m values and the MPTBh and MPTBp compounds), twins and defects.

The outermost (with respect to the centre of the perovskite-type layer in the MPTBh bronzes) WO_6 octahedra share their corners with three PO_4 tetrahedra and three WO_6 octahedra, the next octahedron shares its corners with one PO_4 tetrahedron and five WO_6 octahedra while other WO_6 octahedra are connected to one another only. The degree of distortion of the octahedra (in particular, the scatter of the W–O bond lengths) increases from the centre of the layer towards its periphery, being consistent with the increase in the formal oxidation state of the tungsten atoms calculated using data on the W–O bond lengths. In contrast to this, the average number of conduction electrons increases on going towards the centre of the layer.

All cations (sodium, potassium and lead) occupy a part of the O_{18} cavity near the phosphate groups. As the cation size increases, the average A–O distance also increases (2.68, 2.74 and 2.83 Å for Na, Pb and K, respectively), which is due to distortion of the perovskite-type layer. Positions of the sodium and lead cations differ only slightly. The decrease in the tilt angle of WO_6 octahedra in the Pb-containing structure was ascribed to the increase in the A–O bond lengths and to the steric effect of the lone electron pair whose location was established by Roussel *et al.*[51] Potassium cations are characterised by the smallest scatter of the K–O distances.

Arrangement of sodium cations in the MPTBh and MPTBp frameworks can be followed taking the structures of $Na_{1.7}(PO_2)_4(WO_3)_{12}$ (see Ref. 57) and $Na_4(PO_2)_4(WO_3)_8$ (see Ref. 91) as examples. The O_{18} cavities in the MPTBh structure are connected to four identical cavities by large hexagonal windows and by small rhombohedral windows delimited by two WO_6 octahedra and two PO_4 tetrahedra. The O_{18} cavities in the MPTBp structure are linked to four identical cavities by pentagonal windows. The surface areas of cavities are much larger than those of windows. One half of the cavity is the same for both MPTBh and MPTBp compounds while the other half can be matched by rotation about a twofold axis. On average the corresponding O–O distances in two O_{18} cavities differ by about 1.6%. In both cases the sodium ion is bound to oxygen atoms of the phosphate groups; usually, this ion is treated as an octacoordinate species (for comparison with the potassium-containing MPTB). In this case, the sodium atoms occupy significantly different positions and the scatter of the Na–O bond lengths is rather large. In the $Na_{1.7}(PO_2)_4(WO_3)_{12}$ bronze the sodium ion is displaced from the cavity centre by 1.11 Å; four Na–O bond lengths lie between 2.45 and 2.64 Å while the other four Na–O bond lengths fall within the interval 2.85 to 3.02 Å. In the $Na_4(PO_2)_4(WO_3)_8$ structure the coordination number of the sodium atom decreases to six. The edge-sharing distorted pentagonal pyramids NaO_6 form zigzag chains running along the [010] direction with a Na–Na separation of 3.211 Å (Fig. 8).[91] In the MPTBp structure the sodium ion is displaced from the centre of the O_{18} cavity by 1.5 Å, seven Na–O bond lengths are in the range from 2.37 to 2.64 Å while the eighth Na–O bond length is equal to 2.82 Å.

Table 7. Crystallographic characteristics of the compounds $A_x(PO_2)_4(WO_3)_{2m}$ with $m = 4-7$ and $A_x(P_2O_4)_2(WO_3)_{2m}$ with $m = 4-10$ obtained from single-crystal X-ray diffraction studies.

Composition	m	Space group	Unit cell parameters				Ref.
			a /Å	b /Å	c /Å	angle /deg	
Compounds $A_x(PO_2)_4(WO_3)_{2m}$							
$K_{0.84}P_4W_8O_{32}$	4	$P2_1/m$	6.6702(5)	5.3228(8)	8.9091(8)	$\beta = 100.546(7)$	8, 13, 16, 25, 53, 58
$Na_4P_4W_8O_{32}$	4	$P2_1/m$	6.6065(2)	5.2711(2)	8.8898(2)	$\beta = 99.5898(2)$	91
$Na_{1.5}P_4W_{10}O_{38}$	4	$P2_1/c$	6.6702(5)	5.277(4)	17.788(11)	$\beta = 99.64(5)$	33, 57, 86, 92
$K_{2.01}P_4W_{10}O_{38}$	6	$P2_1/m$	6.6736(2)	5.3543(3)	11.9005(5)	$\beta = 92.615(3)$	25, 41
$Na_{1.7}P_4W_{12}O_{44}$	6	$P2_1/c$	6.588(2)	5.291(1)	23.775(17)	$\beta = 93.47(4)$	37, 56, 57, 86
$K_{1.4}P_4W_{14}O_{50}$	7	$A2/m$	6.660(2)	5.3483(3)	27.06(5)	$\beta = 97.20(2)$ $\alpha = 89.62(1)$	8, 59
$Na_{1.7}P_4W_{14}O_{50}$	7	$A\bar{1}$	6.575(2)	5.304(1)	27.076(3)	$\beta = 96.17(1)$ $\gamma = 90.26(1)$ $\alpha = 90.208(6)$	27, 57
$Pb_{0.66}P_4W_{14}O_{50}$	7	$A1$	6.6015(3)	5.3156(4)	27.039(2)	$\beta = 96.757(5)$ $\gamma = 89.867(5)$	93
Compounds $A_x(P_2O_4)_2(WO_3)_{2m}$							
$RbP_4W_8O_{32}$	4	$A2/m$	10.181(6)	7.519(1)	17.156(4)	$\beta = 113.32(3)$	94
$KP_4W_{10}O_{38}$	5	–	11.061(1)	7.500(1)	17.133(2)	$\beta = 93.78(2)$	60
$RbP_4W_{10}O_{38}$	5	–	11.091(2)	7.522(2)	17.140(2)	$\beta = 93.78(1)$	60
$KP_4W_{12}O_{44}$	6	$A2/m$	14.006(2)	7.530(2)	17.056(2)	$\beta = 114.30(1)$	34, 60
$RbP_4W_{12}O_{44}$	6	$A2/m$	13.991(3)	7.530(1)	17.122(2)	$\beta = 114.22(1)$	61
$BaP_4W_{12}O_{44}$	6	$A2/m$	14.103(3)	7.494(1)	17.027(5)	$\beta = 114.19(1)$	23
$KP_4W_{14}O_{50}$	7	$P2_1/c$	14.618(4)	7.508(3)	17.098(4)	$\beta = 98.99(2)$	34, 60
$RbP_4W_{14}O_{50}$	7	$P2_1/c$	14.638(4)	7.534(3)	17.070(5)	$\beta = 99.00(2)$	60
$RbP_4W_{14}O_{50}$	7	$P2_1/c$	15.723(4)	7.528(6)	17.118(4)	$\beta = 113.42(2)$	62
$BaP_4W_{14}O_{50}$	7	$A2/m$	14.713(3)	7.484(2)	17.175(7)	$\beta = 99.41(3)$	23
$KP_4W_{16}O_{56}$	8	$P2_1/c$	16.208(8)	7.540(4)	17.087(8)	$\beta = 93.92(4)$	22
$RbP_4W_{16}O_{56}$	8	$P2_1/c$	16.209(11)	7.547(3)	17.095(7)	$\beta = 93.99(4)$	22
$RbP_4W_{16}O_{56}$	8	$P2_1/c$	16.194(3)	7.5438(8)	17.095(4)	$\beta = 93.82(2)$	48
$BaP_4W_{16}O_{56}$	8	$A2/m$	17.910(2)	7.480(2)	17.0606(9)	$\beta = 114.74(1)$	27
$BaP_4W_{16}O_{56}$	8	$A2/m$	18.271(4)	7.491(2)	17.346(4)	$\beta = 117.46(2)$	23
$TlP_4W_{16}O_{56}$	8	$P2_1/c$	16.208(8)	7.540(4)	17.087(8)	$\beta = 93.92(4)$	22
$KP_4W_{18}O_{62}$	9	$P2_1/c$	18.143(2)	7.532(2)	17.120(3)	$\beta = 101.54(1)$	60
$RbP_4W_{18}O_{62}$	9	$P2_1/c$	18.069(2)	7.556(2)	17.163(3)	$\beta = 102.53(2)$	60
$KP_4W_{20}O_{68}$	10	$P2_1/c$	21.386(2)	7.534(2)	16.968(1)	$\beta = 113.57(2)$	60
$KP_4W_{20}O_{68}$	10	$P2_1/c$	19.589(3)	7.5362(4)	16.970(3)	$\beta = 91.864(14)$	22
$RbP_4W_{20}O_{68}$	10	$P2_1/c$	21.395(2)	7.552(3)	17.063(5)	$\beta = 113.93(3)$	60
$BaP_4W_{20}O_{68}$	10	$A2/m$	23.193(4)	7.487(2)	17.175(7)	$\beta = 99.41(3)$	23

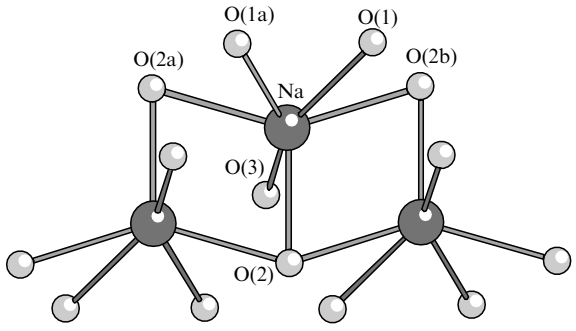


Figure 8. $(NaO_5)_\infty$ chains in the structure of $Na_4(PO_2)_4(WO_3)_8$.

4. Diphosphate tungsten bronzes

Diphosphate tungsten bronzes with hexagonal and pentagonal channels are described by a general formula $A_x(P_2O_4)_2(WO_3)_{2m}$ (A = K, Rb, Cs, Tl, Ba, *etc.*) with integer m values ($4 \leqslant m \leqslant 10$). The frameworks of the simplest members of the DPTB family, compounds $A_x(P_2O_4)_2(WO_3)_4$ (A = Rb, Tl, Ba), contain infinite chains built of ReO_3-type WO_6 octahedra running along the [001] direction of an orthorhombic unit cell. The chains are linked together by diphosphate units. As a result, octagonal channels with a large cross section running along the [001] direction are formed (Fig. 9 *a*); channels with a smaller cross section run along the [010] direction (Fig. 9 *b*). The DPTBs with $m \geqslant 4$ contain characteristic hexagonal channels extending along the [010] direction (see Fig. 1 *d*).

Ordering of cations in the cavities was studied[95] by X-ray diffuse scattering taking the bronze $Cs_{1-x}(P_2O_4)_2(WO_3)_4$ as an example. At 298 K, Cs^+ ions are locally ordered in the lattice along the direction of the channel; however, no correlation between the arrangements of these ions in adjacent channels was found. The period of one-dimensional incommensurate concentration waves depends on stoichiometry with respect to Cs^+ cations. At low temperatures, the degree of intrachannel ordering of Cs^+ cations increases and interchannel ordering appears. Kinetic effects preclude long-range three-dimensional ordering even at low temperatures. Due to the phase shift between the concentration waves of Cs^+ cations in different channels their electrostatic repulsion is minimum. Occurrence of Anderson-type transition in $Cs_{1-x}P_8W_8O_{40}$ (at small x) due to the change in the degree of disorder of ceasium was confirmed by the character of the temperature dependence of electrophysical properties.[95]

In the structure of $(WO_3)_6(P_2O_4)_2$ three nonequivalent WO_6 octahedra differ in the number of bonds with other WO_6 octa-

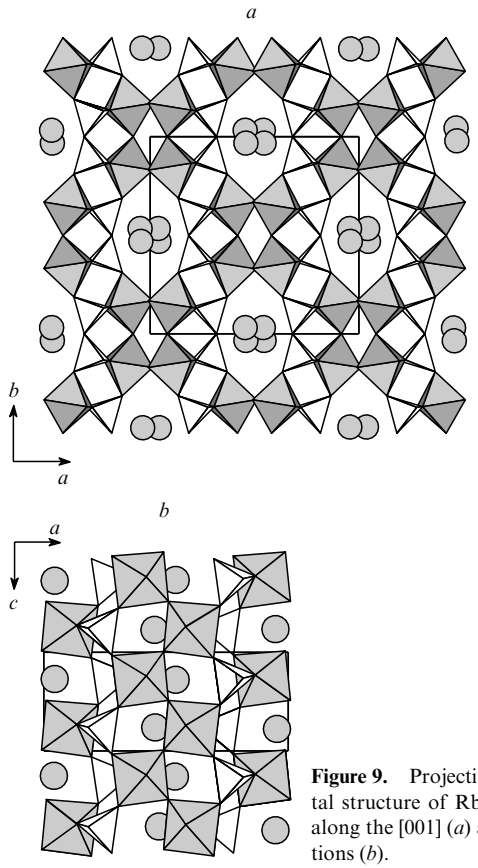


Figure 9. Projections of the crystal structure of $Rb(P_2O_4)_2(WO_3)_4$ along the [001] (*a*) and [010] directions (*b*).

hedra and PO_4 tetrahedra, which equals (5 + 1), (4 + 2) and (3 + 3), respectively. The magnitudes of displacement of the tungsten atoms from the centre of gravity of the octahedron and difference of the W—O bonds in the octahedra increase as the number of bonds with tetrahedra increases. In contrast to all other phosphate tungsten bronzes the structure of $(P_2O_4)_4(WO_3)_{12}$ comprises zigzag-shaped W_6O_{28} chains connected through not only the diphosphate units (P_2O_7) but also immediately through oxygen atoms to form a three-dimensional framework. The structure can be described as a ReO_3-type framework in which one of the four MO_6 octahedra is replaced by the diphosphate unit. Infinite perovskite-type W_3O_{14} ribbons running along the [001] direction are shown in Fig. 10. Two types of channels, *viz*., pentagonal and distorted hexagonal ones extend along the [001] direction (Fig. 11). Three types of face-sharing cavities delimited by thirteen, fourteen and fifteen oxygen atoms can be distinguished in the structure. The O_{13} cavities are formed by six WO_6 octahedra and three PO_4 tetrahedra while O_{14} cavities are formed by six octahedra and two diphosphate units. Elongated O_{15} cavities are formed

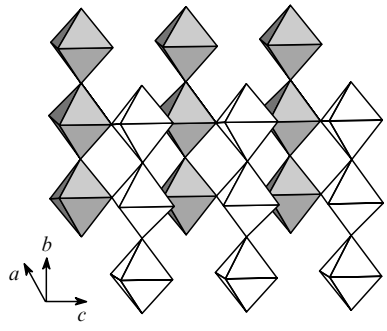


Figure 10. $(W_3O_{14})_\infty$ chains in the structure of $(P_2O_4)_2(WO_3)_6$.

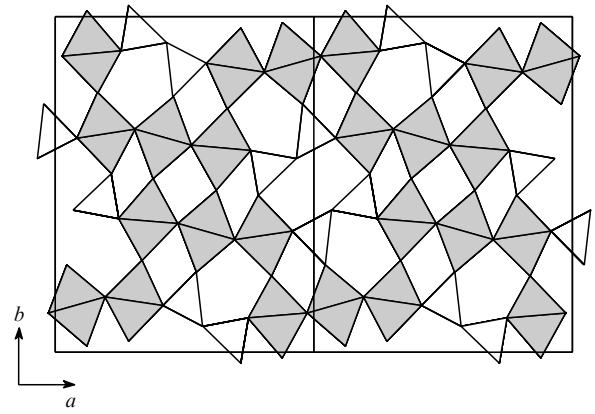


Figure 11. Projection of the crystal structure of $(P_2O_4)_2(WO_3)_6$ along the [001] direction.

by five octahedra and three diphosphate groups. Perovskite-type cavities O_{12} also exist.

The unit cell parameters of the DPTBh compounds with even *m* values ($m > 6$) in the standard setting are [64]

$$a_{\mathrm{DPTBh}} \approx K + 0.5\ a_{\mathrm{per}}\, m,$$

$$b_{\mathrm{DPTBh}} = 2\, a_{\mathrm{per}},$$

$$c_{\mathrm{DPTBh}} = \sqrt{2}\, a_{\mathrm{per}},$$

where $K \approx 2.6$ Å, $\beta \approx 116.6^\circ$.

It should be noted that only the parameter *a* depends on *m* and is related to the layer thickness. For the DPTBh compounds with odd *m* values the unit cell parameters are as follows:[68]

$$a_{\mathrm{DPTBh}} \approx K + a_{\mathrm{per}}[1 + 0.25(m-1)^2],$$

$$b_{\mathrm{DPTBh}} = 2\, a_{\mathrm{per}},$$

$$c_{\mathrm{DPTBh}} = \sqrt{2}\, a_{\mathrm{per}},$$

where $K \approx 2.6$ Å, $\beta \approx 116 - \omega$, $\omega = \arctan[2/(m+1)]$.

Stacking of layers of the same thickness along the *a* direction leads to monoclinic symmetry of the structure. The unit cell parameters of DPTBh, obtained using X-ray diffraction and phase analyses are listed in Table 7.

The diphosphate tungsten bronzes with pentagonal channels were not synthesised as individual phases; however, DPTBp microcrystals containing non-parallel domains with ReO_3-type structure of different thickness (with large *m* values) were found by HRTEM. The tungsten diphosphate WP_2O_7 (see Ref. 96) can be considered as a zeroth member of this class of DPTBs ($m = 2$). Its framework comprises isolated octahedra and zigzag channels with pentagonal windows.

5. Structural defects in phosphate tungsten bronzes

Phosphate tungsten bronzes have been the subject of intensive HRTEM studies. Using this method, it is impossible to reveal small distortions of polyhedra in a real structure with respect to the ideal structural type; however, it is possible to determine non-stoichiometric defects, intergrowth phases, domains and changes in the content of inserted cations in channels.

Structural defects in MPTBs can be divided into two groups. The first group of defects is due to the distribution of planes built of phosphate groups with respect to layers built of the WO_6 octahedra. The second group of defects is due to distribution of PO_4 groups within the phosphate planes.

Electron micrographs of the MPTBs with $m = 4 + 6$ and $m > 12$ usually exhibit certain intergrowth phases of different members of this family of compounds. Bronzes with $m > 13$ were not synthesised as regular single crystals. The compound with $m = 5$ behaves in an unusual manner compared to other phosphate bronzes.[23, 59, 64, 86] Usually, the number of octahedra in the

defect layer approaches that in the main phase. The intergrowth phases can form in both the phosphate [36, 37, 59, 64] and the oxide bronzes in which a shear deformation is possible.

The MPTBh crystals exhibit two kinds of growth defects, (i) separation of the crystal into two regions and (ii) growth of small domains of different thickness on the crystal faces.[57] Often, these domains are somewhat disoriented relative to the main part of the crystal and separated by a clearly seen boundary. In some cases, small domains are poorly crystallisable or amorphous.

A model for connection of these domains through a coherent boundary involving PO_4 tetrahedra, P_2O_7 units in the eclipsed conformation [similar to those found in the structure of $(P_2O_4)_2(WO_3)_6$, see Ref. 97] and edge-sharing WO_6 octahedra was proposed.[57] The boundary is nearly parallel to the hexagonal channel. This model cannot be considered as exclusive; however, structural units employed by the model, *viz.*, the PO_4 and P_2O_7 groups and the edge-sharing WO_6 octahedra are available at any point of the domain boundary.

Changes in the order of alternation of PO_4 tetrahedra and WO_6 octahedra cause two types of defects. Characteristic of the first type of defects is the appearance of additional hexagonal or pentagonal channels. They are observed in the perovskite-type layers containing more than thirteen octahedra [23] and appear only in a part of the layer. The contrast produced by these channels is somewhat different from that produced by the matrix (due to distortions in the framework region adjacent to the defect); however, the content of cations in these channels cannot be determined with certainty. If additional channels in crystals pass throughout the layer, two adjacent layers characterised by small m values appear in the matrix with large m value. This type of defects was found only in the sodium-containing MPTBh.

Additional pentagonal channels characteristic of the MPTBp compounds can appear at the boundary between two MPTBh domains with different orientation of WO_6 octahedra. Correspondingly, hexagonal channels typical of the MPTBh compounds can appear at the boundary between two domains in the MPTBp crystal. A quite rare case is a shear defect along the direction perpendicular to the channel axes.

The potassium- and sodium-containing MPTBh compounds with relatively high alkali metal contents ($x \approx 2$ for K and $x = 3$ for Na) exhibit local variations of the cation concentrations, which lead to distortion of the framework and manifest themselves in periodic changes in the contrast of hexagonal channels.

The nature of cations residing in hexagonal channels affects both the homogeneity region and the structure of the MPTBh compounds. Sodium-containing MPTBh compounds are more stable than their potassium-containing analogues. The sodium-containing bronzes are characterised by a greater variety of defects; a compound with $m = 5$ was stabilised.

A number of the diphosphate tungsten bronzes $Ba_x(P_2O_4)_2(WO_3)_{2m}$ were studied by X-ray diffraction analysis and electron microscopy. Electron diffraction studies showed that, in contrast to the DPTBs containing alkali metal cations, the barium-containing DPTBs exhibit the A-type of the Bravais lattice, superstructural reflections and higher stability. These differences are due to the large covalent component of the bonds between barium and oxygen atoms of the framework. Many $Ba_x(P_2O_4)_2(WO_3)_{2m}$ crystals are characterised by irregular intergrowth. At the same time, ordered intergrowth were observed for the bronzes with $m = 8$ and 9.

IV. Electronic structure

The electronic structures of phosphate tungsten bronzes were calculated by the extended Hückel method. This semiempirical approach is suitable for a more or less satisfactory description of the energy bands of crystals under study but does not allow a reliable geometry optimisation. The research strategy involves analysis of the model fragments (either finite or infinite) of a crystal structure as they become more complicated. To make the electronic structure calculations more exact, information on the band structure of the model systems is used along with the structural data obtained for real compounds.

1. Electronic structure calculations of diphosphate tungsten bronzes

The crystal structure of the first member of the DPTB series, $Cs_{0.5}(P_2O_4)_2(WO_3)_4$ ($m = 2$), is built of isolated W_4O_{18} chains. This compound is expected to possess quasi-one-dimensional electronic properties. The electron count is 1.125 d electrons per tungsten atom and 4.5 d electrons per W_4O_{18} unit. The t_{2g}-levels of $Cs_{0.5}(P_2O_4)_2(WO_3)_4$ are by and large identical to those of an ideal W_4O_{18} chain. The presence of two chains in the unit cell causes a doubling of the bands with a small splitting in each pair of bands. The main feature of the t_{2g}-bands of $Cs_{0.5}(P_2O_4)_2(WO_3)_4$ is that the Fermi level crosses a one-fourth filled one-dimensional delocalised band, whereas the fully filled localised bands and the unfilled delocalised bands are above and below the Fermi level, respectively.[7, 68]

The electronic structure of $Cs_{0.5}(P_2O_4)_2(WO_3)_4$ (see Refs 7, 66 and 67) is similar to that of the lithium bronze $Li_{0.9}Mo_6O_{17}$. In both compounds d electrons are localised within M_4O_{18} (M = W, Mo) chains that are connected in a different way, namely, through diphosphate groups in the former and through Mo_4O_{14} chains built of corner-sharing MoO_6 octahedra and MoO_4 tetrahedra in the latter case. The W_4O_{18} chains in $Cs_{0.5}(P_2O_4)_2(WO_3)_4$ are shielded more weakly than the Mo_4O_{18} chains in $Li_{0.9}Mo_6O_{17}$, so that the conduction electrons are more susceptible to the electric fields created by cations.

Thus, order–disorder transitions of the caesium cations can influence the conducting properties of bronzes. Partial interchannel ordering of cations is observed at a temperature close to the metal–semiconductor transition temperature. Probably, an increase in the resistivity at 24 K is due to the CDW created as a result of one-fourth filling of the one-dimensional bands.[7] As the electron density in the partially filled delocalised bands increases, the shielding (see above) also increases and the conduction electrons become less susceptible to the electric fields created by cations. The $Tl_yCs_x(P_2O_4)_2(WO_3)_4$ phases with $x + y > 0.5$ are isostructural to $Cs_{0.5}(P_2O_4)_2(WO_3)_4$; here, the high-temperature resistivity maximum at 160 K indicating a transition to the CDW state disappears as the sum $x + y$ increases.[7]

The three-dimensional framework of $(P_2O_4)_2(WO_3)_6$ (a DPTB with $m = 3$) contains a system of corner-sharing WO_6 octahedra. Zigzag W_6O_{28} chains are linked by $W'''O_6$ octahedra. According to Zachariasen-type group structure analysis of the W–O bond lengths, the oxidation states of the tungsten atoms W′, W″ and W‴ are 5.19, 5.10 and 5.71, respectively. The band structure of the $W_{12}O_{48}$ framework is similar to that of an isolated W_6O_{28} chain except for the delocalised π-bands in $W_{12}O_{48}$ that cross the Fermi level in all three directions. Therefore, π-orbitals of the $W'''O_6$ octahedra provide not only intrachain but also interchain π-interaction. Therefore, the bronze $(P_2O_4)_2(WO_3)_6$ must possess a three-dimensional metallic conductivity, which was confirmed experimentally. The Zachariasen-type analysis showed that the partially filled delocalised bands are to a great extent composed of the orbitals of the W′ and W″ tungsten atoms.

The $(P_2O_4)_2(WO_3)_6$ bronze significantly differs from the purple bronze $Li_{0.9}Mo_6O_{17}$ in the number of d electrons in the M_4O_{18} (M = Mo, W) chain. Namely, in $Li_{0.9}Mo_6O_{17}$ there are 5.8 electrons per formula unit of the M_4O_{18} chain and the lower lying bands are completly filled, while in the tungsten bronze there are only four electrons and both bands (π and δ) are partially filled. According to calculations, $(P_2O_4)_4(WO_3)_{12}$ must behave as a one-dimensional metal provided that the Fermi level is higher than the π-band upon filling of bands with additional electrons. According to experimental data, the $(Li,Na)_x(P_2O_4)_2(WO_3)_6$ ($x < 0.5$) bronzes containing up to five electrons per formula unit in both (π and δ) bands [7, 67] exhibit a three-dimensional metallic conductivity. Thus, group-structure analysis of the systems $Li_{0.9}Mo_6O_{17}$

and $(P_2O_4)_2(WO_3)_6$ reveals a similar pattern of the distribution of d electrons but different conductivity. This is due to the fact that two types of different-dimensionality bands correspond to the same energy. In these cases, the dimensionality of conductivity strongly depends on the degree of band filling.

For the DPTB compound with $m = 4$, layers built of corner-sharing WO_6 octahedra are similar to Mo_4O_{15} layers in the Magnéli phase Mo_8O_{23}. However, in these structures layers are connected in a different manner, *viz*., through diphosphate groups in the DPTB compound and by Mo_4O_{14} chains built of edge-sharing MoO_6 octahedra in Mo_8O_{23}. Real DPTBs have more complex structures because connection of the layers of WO_6 octahedra by P_2O_7 groups causes small distortions of the octahedra and leads to a unit cell four times larger than that of an ideal W_4O_{15} layer. The average valence corresponding to the oxidation state of tungsten in DPTBs increases with the layer thickness, being equal to $[6-(8+x)/4m]$ in the $(P_2O_4)_2(WO_3)_{2m}$ compounds. At $m = 4$, the number of d electrons per tungsten atom equals 0.625, which is close to the value of 0.5 obtained from calculations for molybdenum atoms in a Mo_4O_{15} layer of the Mo_8O_{23} structure. Therefore, these two systems are structurally similar and exhibit similar electrical properties. No alternation of short and long O–Mo–O bonds along the *b* direction occurs in DPTBs (in contrast to Mo_8O_{23}), so all three t_{2g}-orbitals of tungsten atoms can form low-lying t_{2g}-bands.

The band structures of an ideal W_4O_{17} chain and W_4O_{15} layer have also been calculated. The lowest-lying d-type energy states of the W_4O_{17} chains are four localised bonding δ-bands composed of x^2-y^2-orbitals and eight delocalised π-bands. Four of the delocalised bands are nearly degenerate. The dispersion relations for the t_{2g}-bands along the W_4O_{17} chain of the W_4O_{15} layer are similar to those calculated for a single chain except for the splitting of the four degenerate bands into two groups. The x^2-y^2 orbitals can be involved in interchain π-antibonding interaction and, hence, form a band that is delocalised along the *c* direction. In addition, there are bands originating from the antibonding interaction of the metal d-orbitals with the oxygen p-orbitals along the *b* direction.

The Fermi level calculated for 2.5 electrons in the unit cell crosses the δ- and π-bands originating from the interaction of AOs along the *c* and *b* axes, respectively.[7] Therefore, the system must behave as a two-dimensional metal, *i.e*., possess a metallic conductivity in two directions. However, the Fermi level crosses these bands in such a way that the conductivity along the *b* direction is higher than along the *c* direction. It should be noted that the two-dimensional metallic character of this system is due to the presence of two one-dimensional bands in two mutually perpendicular directions rather than essentially two-dimensional bands.

The band structures calculated for actual W–O layers in $Rb_2(P_2O_4)_2(WO_3)_8$, $Rb_{0.9}(P_2O_4)_2(WO_3)_{12}$ and $Rb_{0.87}(P_2O_4)_2 \cdot (WO_3)_8$ are qualitatively similar to the band structures of an ideal W–O layer. More complex band structure can be a consequence of the doubling of the unit cell (doubling of the parameters *b* and *c*). Hence, all these systems must be two-dimensional metals with the highest conductivity along the *b* direction, which is consistent with experimental data.

A number of bands exhibit a plateau in the vicinity of the Fermi level, which indicates a high density of states. The Fermi level population, $n(E_F)$, can be changed by increasing or decreasing its energy. The increase in $n(E_F)$ can be responsible for the observed increase in the conductivity of both electron-deficient and electron-enriched systems $K_xRb_y(P_2O_4)_2(WO_3)_{12}$ $(x + y < 1)$ and $KSn_x(P_2O_4)_2(WO_3)_{12}$ $(x > 0)$, respectively, compared to the conductivity of $K(P_2O_4)_2(WO_3)_{12}$.[66,67] However, a theoretical model[66] predicts an increase in the conductivity only for the electron-deficient systems $A_{1-x}(P_2O_4)_2(WO_3)_{14}$ $(x > 0)$.

2. Electronic structure calculations of monophosphate tungsten bronzes

The electronic properties of $P_4W_4O_{20}$ differ from those of other MPTBp compounds with $m > 2$. The crystal structure of $P_4W_4O_{20}$ contains no perovskite-type layers; it comprises only the zigzag W_2O_{10} chains built of corner-sharing octahedra. Lithium–molybdenum bronze $Li_{0.9}Mo_6O_{17}$ contains similar Mo_2O_{11} chains. The energy level diagram calculated for $P_4W_4O_{20}$ is similar to that obtained for $Li_{0.9}Mo_6O_{17}$ and exhibits both localised (in *ab* planes) and delocalised (along *c* axis) t_{2g}-bands formed as a result of the interaction of d electrons of tungsten atoms. The t_{2g}-bands are filled with two d electrons (two tungsten(V) atoms in the W_2O_{10} chain per unit cell). The last band is nearly half-filled, while the nearly degenerate localised bands are one-fourth filled. Calculations also predicted a magnetic moment created by electrons in the narrow bands, metallic properties of the compound and its electronic instability.

Perovskite-type layers in the MPTBs with $m > 2$ are characterised by nonuniform distribution of d electrons whose concentration increases from the centre of the layer towards its periphery.

The monophosphate tungsten bronzes are two-dimensional metals similar to their structural analogues, γ-Mo_4O_{11} and η-Mo_4O_{11}. The transport properties and electronic instabilities of the W–O and Mo–O layers in the Magnéli phases are different. The Mo–O layers have a larger number of d electrons due to the difference in the oxidation state of the atom in a tetrahedral environment [Mo(VI) in the Magnéli phases and P(V) in the MPTBs]. Changes in the topology of the Fermi surface as a function of the number of d electrons in the unit cell and the thickness of the perovskite-type layer have been studied.[7] The electronic band structures of the MPTBs were calculated by the extended Hückel tight binding method using the modified Wolfsberg–Helmholtz approximation.[6,7]

The electronic band structures of different MPTBs obey an identical pattern, being similar to the band structure calculated for an ideal layer built of regular WO_6 octahedra. An example of this layer is provided by, *e.g*., a W_4O_{16} layer with W–O distances of 1.916 Å. The average oxidation state of the tungsten atoms in $(PO_2)_4(WO_3)_{2m}$ is $(6m-2)/m$. Therefore, each layer of WO_6 octahedra contains two d electrons per unit cell irrespective of *m* value. In the $A_x(PO_2)_4(WO_3)_{2m}$ bronzes containing monovalent cations each layer has $(2 + x/2)$ electrons in the unit cell to fill the t_{2g}-bands (Fig. 12).[67] Two Magnéli phases, γ-Mo_4O_{11} and η-Mo_4O_{11}, are characterised by $N = 4$, the $A_2(PO_2)_4(WO_3)_{2m}$ compounds are characterised by $N = 3$ while $N = 2$ for the MPTBp compounds. At $N \leqslant 4$, only two bottom bands are partially filled, one of them being one-dimensional while the other (consisting of two subbands) is a two-dimensional one.

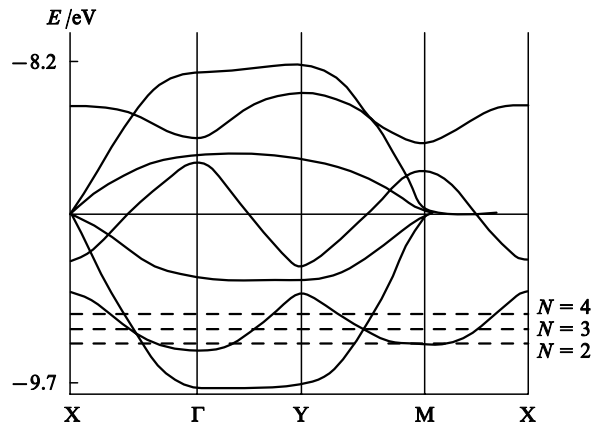


Figure 12. Dispersion relations for the t_{2g}-bands in a perfect W_4O_{16} layer. Dashed lines denote the Fermi levels at different numbers of d electrons in the unit cell (*N*).

Table 8. Peierls transition temperatures and the modulation wave vectors of some MPTBp compounds.

m	T_P /K		Modulation wave vector $\boldsymbol{q}^{(m)}$ (see [a])	Ref.
	T_{P1}	T_{P2}		
4	80(1)	52(1)	$\boldsymbol{q}_1^{(4)} = [0.330(5), 0.295(5)]$, $\boldsymbol{q}_2^{(4)} = [0.340(5), 0.000(5)]$	14, 47, 99 – 102, 104, 106
5	83(5)	60(2)	$\boldsymbol{q}_1^{(4)} = [0.32(1), 0.29(1), 0.0(1)]$, $\boldsymbol{q}_2^{(4)} = [0.36(1), 0.00(5), 0.0(1)]$	98
4 + 6	158(2)	–	$\boldsymbol{q}_1^{(4)} = [0.330(5), 0.295(5)]$, $\boldsymbol{q}_2^{(4)} = [0.33(4), 0.00(4)]$	103, 104
6	120(1)	62(1), ~ 30 [b]	$\boldsymbol{q}_1^{(6)} = [0.385(5), 0.000(5)]$, $\boldsymbol{q}_2^{(6)} = [0.310(5), 0.295(5)]$, $\boldsymbol{q}_3^{(6)} = [0.29(2), 0.11(2)]$	14, 18, 33, 100 – 102, 104, 106
7	183 – 188	47 – 60	$\boldsymbol{q}_1^{(7)} = [0.260(3), 0.073(3), 0.27(5)]$, $n = 1 - 7$	18, 19 100, 101, 104, 106
	188(1)	60(1)	$n\boldsymbol{q}_2^{(7)} = n[0.12(1), 0.03(1), 0.15(5)]$, $n = 1, 3, 5$	
8	≈220	~200	$\boldsymbol{q}_1^{(8)} = [0.47(2), 0.02\ (1), 0.15(10)]$, $n\boldsymbol{q}_2^{(8)} = n[0.19(2), 0.03(1), 0.15(5)]$, $n = 1 - 6$ (see [c])	104, 105
9	565(5)	330(5)	$\boldsymbol{q}_0^{(9)} = [0.50(1), 0.00(1), 0.0(2)]$, $\boldsymbol{q}_1^{(9)} = [0.17(1), 0.00(1), 0.0(2)]$	104, 105
10 (see [d])	≈450		$\boldsymbol{q}^{(10)}$ (300 K) = [0.43(1), 0.00(1), 0.0(1)], $\boldsymbol{q}^{(10)}$ (300 K) = [0.14(1), 0.00(1), 0.0(1)]	47, 104
11	560(5)	–	$n\boldsymbol{q}^{(11)}(T) = 1, 2, 3$; $\boldsymbol{q}^{(11)}$ (300 K) = [0.43(1), 0.00(1), 0.0(1)]	81
12	535(5)	500(5)	$\boldsymbol{q}_1^{(12)} = [0.12(1), 0.00(2), 0.0(2)]$, $\boldsymbol{q}_0^{(12)} = [0.50(1), 0.00(1), 0.5(2)]$	47, 104, 105
13	550(5)	–	$n\boldsymbol{q}_1^{(13)} = [0.053(8), 0.016(10)]$, $n = 1, 2$;	17, 104, 105
	510(5)	–	$\boldsymbol{q}_0^{(13)} = [0.50(1), 0.00(1), 0.0(2)]$, $\boldsymbol{q}_2^{(13)} = [0.178(8), 0.145(10)]$	
	160(10)	–		
14	≈695 – 730	–	$\boldsymbol{q}_0^{(14)} = [0.50(1), 0.00(1), 0.5(2)]$	104, 105

[a] Presented in units of the reciprocal cell. [b] The T_{P3} value. [c] In the case of short-range order in the crystal. [d] The crystal was doped with 0.2% Ge.

3. The Fermi surfaces

The Fermi surface of an ideal one-dimensional metal consists of two parallel planes separated by the Fermi wave vector $2\boldsymbol{k}_F$. A Peierls transition (metal – insulator transition) causes destruction of this Fermi surface. The Fermi surfaces of quasi-two-dimensional (2D) conductors are of more complex shape.[10] In this case a Peierls transition causes a partial destruction of the Fermi surface; as a consequence, metal – metal transitions are observed. Transitions to the CDW state or between two CDW states are a consequence of the interaction between a phonon and the energy states of conduction electrons. Pre-transitional phenomena observed in the MPTBp compounds above the Peierls transition temperature (T_P) indicate that CDW-type instability is due to the quasi-one-dimensional electronic structure of these compounds. Large flat areas of the Fermi surface which include bands of different orientation can be calculated using the extended Hückel tight binding approximation.[6, 7, 10] X-Ray diffuse scattering experiments [14, 17 – 19, 47, 81, 98 – 106] allowed the Fermi vectors for each quasi-one-dimensional area of the Fermi surface to be determined (Table 8).

The Fermi surface was first imaged by high-resolution photoemission UV spectroscopy in a study of MPTBp compounds with $4 \leqslant m \leqslant 12$.[104] The Fermi surface of $(PO_2)_4(WO_3)_8$ contains quasi-one-dimensional bands,[104, 107] which is consistent with the results of earlier band structure calculations.[66, 67, 108]

V. Electrophysical properties

The electric and magnetic properties of MPTBp polymorphs with $m = 2$ [the α- and β-phases of $(PO_2)_4(WO_3)_4$] were first studied by Kinomura *et al.*[49] Both phases exhibit semiconducting properties in the temperature range 77 – 420 K. The monoclinic β-phase is characterised by higher conductivity. The results of preliminary magnetisation measurements with α-phase and β-phase polycrystals in the temperature interval 77 – 500 K revealed nonzero local magnetic moments.

The magnetic susceptibility (2 – 300 K, in a 5000 G field) and the resistivity (50 – 390 K) of oriented MPTBp single crystals were experimentally studied by Greenblatt *et al.*[52] In this temperature range, the resistivity shows a semiconducting behaviour. At 298 K, the resistivity measured along different crystallographic axes is $R_c = 5 \times 10^{-3}$, $R_b = 4 \times 10^{-2}$ and $R_a = 1 \times 10^{-1}$ Ω cm. At $T < 50$ K, the resistivity is $\geqslant 10^4$ Ω cm. Seebeck effect measurements at 300 K showed electrons as the main type of charge carriers (*n*-type conduction). Experiments revealed a semiconducting rather than the predicted metallic type of conductivity along the *c* axis (though the conductivity at 298 K approaches a value characteristic of metals).

The temperature dependence of the magnetic susceptibility (χ) in the samples exhibits the onset of antiferromagnetic ordering at 15 K. In the temperature range 50 – 300 K the dependence of $1/\chi$ on T obeys the Curie – Weiss law with $\theta = -34.6$ K. The effective magnetic moment in this temperature range is 0.88 μ_B. The large deviation of this dependence from the linear one at $T < 50$ K is likely due to the change in the type of magnetic exchange interaction upon structural phase transition.

A large anisotropy of the Neel temperature (T_N) was found along the *b* direction ($T_N \approx 16$ K), along the *c* direction ($T_N \approx 20$ K) and along the *a* direction at low temperatures the temperature dependence of χ exhibits a plateau with $\chi_{max} = 1.12 \times 10^{-2}$ cm^3 mol^{-1} at 4.6 K. Taking into account a rather low activation energy for conductivity along the *a* axis ($E_a = 0.084$ eV at 50 – 200 K), the conductivity can be described in terms of the hopping of small polarons in the narrow conduction bands originating from the overlap of 5d-orbitals of the tungsten atom and 2p-orbitals of the oxygen atom.

The crystal structure of the monophosphate tungsten bronze $(PO_2)_4(WO_3)_4$ comprises isolated chains built of WO_6 octahedra with the lowest (for this class of compounds) oxidation state of tungsten. Along $(WO_5)_\infty$ chains (*c* axis direction) the magnetisation is much lower while the conductivity is much higher than along other axes.

CDW-type electronic instabilities are also possible in bronzes. At 298 K, high semimetallic conductivity along one-dimensional chains built of WO_6 octahedra implies a transition to the metallic state, *i.e.*, a CDW-type instability at $T > 390$ K, as was predicted by Canadell and Whangbo.[109]

At present, the properties of the $(PO_2)_4(WO_3)_{2m}$ bronzes with $4 \leqslant m \leqslant 14$ have been a subject of most intensive studies.[3, 10, 88, 99] It was established that the critical temperature of Peierls transition and the resistivity at room temperature increase with the thickness of the layer of WO_6 octahedra. This is consistent with the simple models proposed for the monophosphate tungsten bronzes with $m = 4 - 12$.[16, 84, 98] At the same time, the MPTBp compounds with

$m = 4$ and 6 are treated as typical CDW-compounds while the compounds with $m = 7$ exhibit anomalous electrophysical properties.

The electrophysical properties of the bronzes $(PO_2)_4(WO_3)_{2m}$ are closely related to the character of the Fermi surface. Some studies take into account the role of electron – phonon interaction. In particular, a rather high resistivity at room temperature should be ascribed to an increase in the contribution of electron – phonon (or electron – electron) interaction, which can be due to the presence of the CDW satellites corresponding to anharmonic CDW modulation. With allowance for this fact the electrophysical properties of certain phosphate tungsten bronzes should be described using the bipolaron model rather than the traditionally used CDW model.[110]

The results of studies on the bronzes with $m = 10$ and 12 indicate that the critical temperatures of transitions to the CDW state increase as the m value increases. It should be noted that crystals were grown using glass-forming oxides. This was accompanied by doping the crystals (with *e.g.*, germanium). Due to the different electronic structures of the impurity and the host atoms it is possible to change the density of states at the Fermi level. A Ge $\leftrightarrow$ P substitution of tetrahedral positions was also proposed;[47] we believe that the Ge $\leftrightarrow$ W substitution [38] is also possible, though the impurity concentration is rather low and no significant changes in the temperature of transition to the CDW state are expected.

An increase in the resistivity at room temperature with increasing m is comparable with the decrease in the charge carrier concentration evaluated using a simple Drude model. The average number of electrons in the samples with $m = 4$ and 12 was estimated at 7×10^{27} and 3×10^{27} m^{-3}, respectively. However, this provides no explanation for the fact that the resistivity increases by two orders of magnitude in the temperature interval from 4 to 300 K and undoubtedly indicates that the band theory, as applied to the crystals in question, is of limited use. This is confirmed by the conductivity of these crystals at room temperature ($\sigma_{300\ K} = 10^2\ \Omega\ cm^{-1}$ for $m = 12$), which approaches the lowest possible value of the metallic type conductivity. It should be noticed that the electrophysical properties of the compounds $(PO_2)_4(WO_3)_{2m}$ with large m values can be described in terms of the theory of Fermi liquid.[108]

Experiments with single crystals of the bronzes with $7 < m \leqslant 12$ showed that the Peierls transition temperatures and the resistivity at room temperature increase as m increases, as is expected in accord with the known models. Diffraction intensity measurements of the CDW satellites for $m = 7$ revealed two transitions at $T_{P1} = 183 - 188$ K and $T_{P2} = 47 - 60$ K. The transition temperatures depend on the method of growth of single crystals (chemical vapour transport reactions or solid-phase synthesis) and on the purity of the starting components. The T_{P1} transition, which is accompanied by considerable changes in the resistivity, seems to be a first-order phase transition.[88]

At $T \leqslant 180$ K, the temperature dependences of the resistivity and intensity of the CDW satellites exhibit a large hysteresis. This means that the CDW state is metastable below T_{P1}. The low-temperature transition affects the transport properties of the compound only after the onset of magnetoresistance at 6 T. This transition was detected during specific heat measurements using a relaxation technique.[17] The enthalpy and entropy of this transition to the CDW state are $\Delta H_{P2} = 220$ J mol^{-1} and $\Delta S_{P2} = 5.5$ J mol^{-1} K^{-1}, respectively.

Based on the X-ray diffraction data, two families of CDW satellites at $\boldsymbol{q}_1 = a^*/2\,(T_{P1} \approx 445\ K)$ and $\boldsymbol{q}_2 = a^*/3\,(T_{P2} = 324\ K)$ were found for the compound with $m = 9$.[85] The temperature dependences show that the resistivity at 300 K and the critical temperatures of transition to the CDW state increase as m increases.

It should be noted that the resistivity ($R_{300\ K}$) increases by two orders of magnitude on going from $m = 4$ to $m = 12$. However, the compound with $m = 7$ exhibits an abnormally high resistivity ($R_{300\ K} = 30$ mΩ cm). The temperature T_P monotonically increases by about an order of magnitude for the whole series of compounds with $4 \leqslant m \leqslant 12$ including the bronze with $m = 7$.[47]

Structural studies confirmed the onset of the CDW state in the $(PO_2)_4(WO_3)_{2m}$ compounds with $m = 10$ and 12 at room temperature. For the compound with $m = 10$ the CDW wave vector [$\boldsymbol{q} = (3/7)a^*$ in the undoped sample] is shifted towards $\boldsymbol{q} = a^*/2$ in the Ge-doped samples.[85]

CDW-satellites with $\boldsymbol{q} = a^*/2$ in these bronzes characterise a phase with $m = 12$. However, the nature of the low-temperature resistivity anomaly in these compounds has not been studied as yet.

The phases with $m = 4$ and 6 are regular and undergo a CDW transition. The MPTBp compound with $m = 7$ possesses anomalous properties. The higher $R_{300\ K}$ value corresponds to strong electron – phonon or electron – electron interaction, which is indirectly confirmed by the presence of the CDW satellite harmonics, which indicate an anharmonic CDW modulation. In this context the phenomenon should be described using the bipolaron model.[107]

X-Ray diffuse scattering data obtained for the phases with $m = 4$ and 6 showed that two different CDWs coexist in the temperature intervals 40 – 60 and 75 – 85 K.[3, 88] The large magnetoresistance at low temperatures along the direction perpendicular to perovskite-type layers was ascribed to the existence of unfilled states on the Fermi surface in the CDW state.[100]

To study how the population of energy levels influences the CDW character, the conductivity, magnetoresistance, Hall effect, thermoelectric power and specific heat were studied using a number of $K_x(PO_2)_4(WO_3)_8$ samples with $0.8 < x < 1.94$ [$K_x(PO_2)_4(WO_3)_8$ is an MPTBh compound].[8] All the compounds studied exhibit anomalous dependences of the Curie temperature (T_c) on x. The $T_c(x)$ curve plotted using the conductivity data for $x = 1.3$ passes through a maximum at $T = 170$ K. Based on the results of X-ray diffraction studies of the samples,[13, 58] the observed $T_c(x)$ dependence can be explained as a manifestation of nonmonotonic behaviour of the density of electronic states upon variation of energy. In contrast to transitions in the undoped monophosphate bronze $(PO_2)_4(WO_3)_8$, transitions in $K_x(PO_2)_4(WO_3)_8$ are not determined by conventional Peierls-type charge density instability and cannot be treated only in the framework of the Bloch – Grüneisen model for collisions between charge carriers and phonons.[8, 16]

VI. Conclusion

The phosphate tungsten bronzes exhibiting unusual electrophysical properties and electronic instabilities are studied by various physical and crystallographic methods. A number of MPTBp compounds forms several CDW states. The properties of the MPTBh and DPTBh compounds strongly depend on the type and concentration of inserted cations, affecting the number of electrons in the partially filled conduction band. Peculiarities of the crystal and electronic structures of these compounds permit independent variation of the thickness of the conducting layer and the degree of filling of the conduction band. This opens up great prospects for targeted design of materials with preset electrophysical properties.

Topology features of the Fermi surface in the phosphate tungsten bronzes are studied using modern quantum-chemical calculations and experimental methods.[89, 104, 111 – 114]

The range of phosphate tungsten bronzes is continuously being extended as a result of elaboration of new methods of synthesis. Systematisation of information on the structure – property relations will be useful for development of software for computer simulation of electrophysical properties of these complex systems.

Recently, the phosphate tungsten bronzes have found some fields of practical application. Materials based on the tungsten and molybdenum oxides are now widely used in electrochromic

cells, optical devices, as secondary batteries, in gas sensors and as catalysts of various processes.[115–130] This is also possible for the phosphate tungsten bronzes that exhibit catalytic activity in some oxidation and isomerisation reactions.[131–133]

The first MOSFET-like device employing the motion of CDW in $Rb_{0.3}MoO_3$ was fabricated recently. However, it is of limited use because a single crystal is used as the working substance.[134]

Particular emphasis is placed on practical applications of the dimensionality effects, in particular, for film heterostructures (single-phase epitaxial films grown by pulse-laser deposition), which exhibit a coherent CDW transport. Nonlinear behaviour of these films in weak electromagnetic fields leads to extremely high dielectric constant (from $>10^8$ at low frequencies to 10^3 at microwave frequencies) and is of considerable interest for modern electronics.[135] At present, no devices employing the phosphate tungsten bronzes are available because of the lack of supported bronze thin films. However, first attempts at obtaining such films have been made by the authors of this review.[136–138]

One can assume that the CDW transition temperatures and the resistance of oriented thin films of the phosphate tungsten bronzes can be controlled by synthesis of layers of specified thickness. This allows fabrication of controllable heterostructures made of these new functional materials using, in particular, lithography techniques. Submicrometre-scale structures and nanostructures based on phosphate tungsten bronzes will also permit implementation of new possibilities in the studies of the influence of the dimensionality on the CDW phenomenon.

References

1. J Bardeu *Phys. Today* **12** 25 (1990)
2. A Ottolenghi, J-P Pouget *J. Phys. I* **6** 1059 (1996)
3. M Greenblatt *Int. J. Mod. Phys. V* **7** 4045 (1993)
4. C Schlenker *Low-Dimensional Electronic Properties of Molybdenum Bronzes and Oxides* (Dordrecht: Kluwer Academic, 1989)
5. G Gruner (Ed.) *Density Waves in Solids, Frontiers of Physics Series* (Reading, MA: Addison Wesley, 1994)
6. E Canadell, M-H Whangbo *Phys. Rev. V* **43** 1894 (1991)
7. E Canadell, M Whangbo *Chem. Rev.* **91** 965 (1991)
8. P Roussel, D Groult, C Hess, Ph Labbe, C Schlenker *J. Phys.: Condens. Mater.* **9** 7081 (1997)
9. J Rouxel (Ed.) *Crystal Chemistry and Properties of Materials with Quasi-one-dimensional Structures* (Dodrecht, Boston, Lancaster, Tokyo: Kluwer Academic, 1986)
10. M-H Whangbo, E Canadell, P Foury, J R Pouget *Science* **252** 96 (1991)
11. S Adams *J. Solid State Chem.* **149** 75 (2000)
12. C Schlenker, C Hess, C Letouze, J Dumas *J. Phys. I* **6** 2061 (1996)
13. J Dumas, U Beierlein, S Drouard, C Hess, D Groult, Ph Labbe, P Roussel, G Bonfait, E Gomez Marin, C Schlenker *J. Solid State Chem.* **147** 320 (1999)
14. C Hess, C Schlenker, J Dumas, M Greenblatt, Z S Teweldemedhin *Phys. Rev. B* **54** 4581 (1996)
15. P Foury, J R Pouget, Z S Teweldemedhin, E Wang, M Greenblatt, D Groult *J. Phys. IV* **3** C2-133 (1993)
16. S Drouard, J Dumas, P Foury, J P Pouget, P Roussel, C Schlenker, D Groult *Synth. Met.* **103** 2636 (1999)
17. J Lehmann, C Schlenker, C Letouze, A Rotger, J Dumas, J Marcus, Z S Teweldemedhin, M Greenblatt *J. Phys. IV* **3** C2–243 (1993)
18. C Hess, C Shlenker, G Bonfait, T Ohm, C Paulsen, D Dumas, Z Teweldemedhin, M Greenblatt, J Marcus, M Almeida *Solid State Commun.* **104** 663 (1997)
19. C Hess, C Shlenker, G Bonfait, J Marcus, T Ohm, C Paulsen, J Dumas, J L Tholence, M Greenblatt, M Almeida *Physica C* **282–287** 955 (1997)
20. Ph Labbe, M Goreaud, B Raveau *J. Solid State Chem.* **61** 324 (1986)
21. S L Wang, C C Wang, K H Lii *J. Solid State Chem.* **82** 298 (1989)
22. J P Giroult, M Goreaud, Ph Labbe, B Raveau *Acta Crystallogr., Sect B: Struct. Crystallogr. Cryst. Chem.* **37** 2139 (1981)
23. B Domenges, M Hervieu, B Raveau, R J D Tilley *J. Solid State Chem.* **54** 10 (1984)
24. M Hervieu, B Domenges, B Raveau *J. Solid State Chem.* **58** 233 (1985)
25. B Domenges, M Hervieu, B Raveau, M O'Keeffe *J. Solid State Chem.* **72** 155 (1988)
26. Ph Labbe, D Ouachee, M Goreaud, B Raveau *J. Solid State Chem.* **50** 163 (1983)
27. M Lamire, Ph Labbe, M Goreaud, B Raveau *J. Solid State Chem.* **71** 342 (1987)
28. E Wang, M Greenblatt *J. Solid State Chem.* **68** 38 (1987)
29. E Wang, M Greenblatt, in *Extended Abstract Papers of the 197th American Chemical Society National Meeting, Dallas, TX, 1989* p. 520
30. C Schlenker, J Dumas, M Greenblatt, S Van Smalen (Eds) *Physics and Chemistry of Low Dimensional Inorganic Conductors. NATO-ASI. Ser. B: Physics* (New York: Plenum, 1996) Vol. 354
31. E Wang, M Greenblatt, I Rachidi, E Canadell, M-H Whangbo *J. Solid State Chem.* **81** 173 (1989)
32. E Wang, M Greenblatt, I Rachidi, E Canadell, M-H Whangbo *J. Solid State Chem.* **80** 266 (1989)
33. E Wang, M Greenblatt, I Rachidi, E Canadell, M-H Whangbo, S Vadlamannati *Phys. Rev. B* **39** 12969 (1989)
34. E Wang, M Greenblatt, I Rachidi, E Canadell, M-H Whangbo, S Vadlamannati *Phys. Rev. B* **40** 11964 (1989)
35. V V Lisnyak, N S Slobodyanik, V Ya Zub *Ukr. Khim. Zh.* **65** 78 (1999)
36. M Hervieu, B Raveau *Chem. Scr.* **22** 117 (1983)
37. M Hervieu, B Raveau *Chem. Scr.* **22** 123 (1983)
38. V V Lisnyak, Candidate Thesis in Chemical Sciences, Kiev National University, Kiev, 2001
39. V V Lisnyak, V S Sudavtsova, N V Stus, M S Slobodyanik, in *The 6th International School-Conference Phase Diagrams in Materials Science, Kiev, 2001* p. 76
40. P Roussel, D Groult, A Maignan, Ph Labbe *Chem. Mater.* **11** 2049 (1999)
41. P Roussel, S Drouard, D Groult, Ph Labbe, J Dumas, C Schlenker *J. Mater. Chem.* **9** 973 (1999)
42. H Mathis, R Glaum, R Gruehn *Acta. Chem. Scand.* **45** 781 (1991)
43. R Gruehn, R Glaum *Angew. Chem., Int. Ed.* **112** 706 (2000)
44. M Lenz, R Gruehn *Chem. Rev.* **97** 2967 (1997)
45. H Mathis, R Galum, R Gruehn, in *7 Vortrastagung der GDCh-Fachgruppe, Festkorperchemie, Bonn, 1994* p. 87
46. R Galum, O Trappe *Das Computerprogramm CVTRANS zur Modellierung Chemischer Transportexperimente* (Gießen: Universität Gießen, 1999)
47. C Schlenker, C Letouze, C Hess, A Rltger, J Dumas, J Marcus, M Greenblatt, Z S Teweldemedhin, A Ottolenghi, P Foury, J P Pouget *Synth. Met.* **70** 1263 (1995)
48. J P Giroult, M Goreaud, Ph Labbe, B Raveau *Acta Crystallogr., Sect. B: Struct. Crystallogr. Cryst. Chem.* **36** 2570 (1980)
49. N Kinomura, M Hirose, N Kumada, F Muto, T Ashida *J. Solid State Chem.* **77** 156 (1988)
50. P Roussel, P Foury-Leylekian, B Domenges, D Groult, Ph Labbe, J-P Pouget *Eur. Phys. J. B* **12** 497 (1999)
51. P Roussel, G Mather, B Domenges, D Groult, Ph Labbe *Acta Crystallogr., Sect. B: Struct. Sci.* **54** 365 (1998)
52. Z S Teweldemedhin, K V Ramanujachary, M Greenblatt *J. Solid State Chem.* **95** 21 (1991)
53. J P Giroult, M Goreaud, Ph Labbe, B Raveau *J. Solid State Chem.* **44** 407 (1982)
54. P Roussel, Ph Labbe, D Groult, B Domenges, H Leligny, D Grebille *J. Solid State Chem.* **122** 281 (1996)
55. P Roussel, Ph Labbe, H Leligny, D Groult, P Foury-Leylekian, J P Pouget *Phys. Rev. B* **62** 176 (2000)
56. A Benmoussa, D Groult, Ph Labbe, B Raveau *Acta Crystallogr., Sect C: Cryst. Struct. Commun.* **40** 573 (1984)
57. B Domenges, M Hervieu, B Raveau *Acta Crystallogr., Sect. B: Struct. Sci.* **46** 610 (1990)

58. S Drouard, D Groult, J Dumas, R Buder, C Schlenker *Eur. Phys. J. V* **16** 593 (2000)
59. B Domenges, M Goreaud, Ph Labbe, B Raveau *J. Solid State Chem.* **50** 173 (1983)
60. M Hervieu, B Raveau *J. Solid State Chem.* **43** 299 (1982)
61. J P Giroult, M Goreaud, Ph Labbe, B Raveau *Acta Crystallogr., Sect. B: Struct. Crystallogr. Cryst. Chem.* **37** 1163 (1981)
62. J P Giroult, M Goreaud, Ph Labbe, B Raveau *Acta Crystallogr., Sect. B: Struct. Crystallogr. Cryst. Chem.* **38** 2342 (1982)
63. M Goreaud, Ph Labbe, B Raveau *J. Solid State Chem.* **56** 41 (1985)
64. B Domenges, M Hervieu, B Raveau *Acta Crystallogr., Sect. B: Struct. Sci.* **40** 249 (1984)
65. E Wang, M Greenblatt *J. Solid State Chem.* **76** 340 (1988)
66. E Canadell, I Rachidi, E Wang, M Greenblatt, M-H Whangbo *Inorg. Chem.* **28** 2455 (1989)
67. E Wang, M Greenblatt, I Rachidi, E Canadell, M-H Whangbo *Inorg. Chem.* **28** 2452 (1989)
68. P Roussel, O Perez, Ph Labbe *Acta Crystallogr., Sect. B: Struct. Sci.* **57** 603 (2001)
69. V V Lisnyak, N V Stus, A M Solomon, in *Anniversary Fedorov Session FS2003, St Petersburg, 2003* p. 57
70. F Berrah, A Leclaire, A Guesdon, M M Borel, J Provost, B Raveau *J. Solid State Chem.* **141** 155 (1998)
71. A Leclaire, M M Borel, J Chardon, B Raveau *J. Solid State Chem.* **130** 48 (1997)
72. A Leclaire, M M Borel, J Chardon, B Raveau *J. Solid State Chem.* **127** 1 (1996)
73. A Leclaire, M M Borel, J Chardon, B Raveau *J. Solid State Chem.* **120** 353 (1995)
74. A Leclaire, M M Borel, J Chardon, B Raveau *J. Solid State Chem.* **124** 224 (1996)
75. A Leclaire, M M Borel, J Chardon, B Raveau *J. Solid State Chem.* **128** 215 (1997)
76. A Leclaire, M M Borel, J Chardon, B Raveau *Mater. Res. Bull.* **31** 1257 (1996)
77. A Leclaire, M M Borel, J Chardon, B Raveau *J. Solid State Chem.* **128** 191 (1997)
78. D Mezaoui, A Laclaire, M M Borel, B Raveau *Z. Kristallogr.* **212** 837 (1997)
79. A Leclaire, M M Borel, D Mezaoui, H Rebbah, B Raveau *C.R. Acad. Sci., Ser. IIc* **323** 679 (1996)
80. D Mezaoui, M M Borel, A Leclaire, H Rebbah, J Provost, B Raveau *J. Solid State Chem.* **136** 305 (1998)
81. P Roussel, Ph Labbe, D Groult *Acta Crystallogr., Sect. B: Struct. Sci.* **56** 377 (2000)
82. P Foury, J-P Pouget *Int. J. Mod. Phys. B* **7** 3973 (1993)
83. P Foury, J-P Pouget, Z Tewldemedihin, E Wang, M Greenblatt *Synth. Met.* **55 – 57** 2605 (1993)
84. P Foury, J-P Pouget, P Roussel, D Groult *Synth. Met.* **103** 2624 (1999)
85. A Ottolenghi, P Foury, J P Pouget, Z S Teweldemedhin, M Greenblatt, D Groult, J Marcus, C Schlenker *Synth. Met.* **70** 1301 (1995)
86. A Benmoussa, Ph Labbe, D Groult, B Raveau *J. Solid State Chem.* **44** 318 (1982)
87. P Foury, J P Pouget, E Wang, M Greenblatt *Synth. Met.* **43** 3973 (1991)
88. P Foury, J P Pouget, E Wang, M Greenblatt *Europhys. Lett.* **16** 485 (1991)
89. J Ludecke, A Jobst, S van Smaalen *Europhys. Lett.* **49** 357 (2000)
90. N V Stus, V V Lisnyak, M S Slobodyanik, in *Proceedings of the 20th European Crystallographic Meeting on Crystallography in Natural Science and Technology, Krakow, 2001* Vol. 1, p. 252
91. N V Stus, V V Lisnyak, M S Slobodyanik *J. Alloys Compd.* **325** 73 (2001)
92. A Benmoussa, D Groult, B Raveau *Rev. Chim. Miner.* **21** 710 (1984)
93. P Roussel, A C Masset, B Domenges, A Maignan, D Groult, Ph Labbe *J. Solid State Chem.* **139** 362 (1998)
94. J P Giroult, M Goreaud, Ph Labbe, B Raveau *Rev. Chim. Miner.* **20** 829 (1983)
95. P Foury-Leylekian, J P Pouget, M Greenblatt, E Wang *Eur. Phys. J. B* **2** 157 (1998)
96. V V Lisnyak, N V Stus, N S Slobodyanik, N M Belyavina, V Ya Markiv *J. Alloys Compd.* **309** 83 (2000)
97. B Domenges, M Goreaud, Ph Labbe, B Raveau *Acta Crystallogr., Sect. B: Struct. Crystallogr. Cryst. Chem.* **38** 1724 (1982)
98. U Beierlein, C Schlenker, J Dumas, D Groult, Ph Labbe, E Balthes, E Steep *Synth. Met.* **103** 2593 (1999)
99. Z S Teweldemedhin, K V Ramanujachary, M Greenblatt *Phys. Rev. B* **46** 7897 (1992)
100. A Rötger, J Lehmann, C Schlenker, J Dumas, J Marcus, Z S Teweldemedhin, M Greenblatt *Europhys. Lett.* **25** 23 (1994)
101. A Rötger, C Schlenker, J Dumas, E Wang, Z S Teweldemedhin, M Greenblatt *Synth. Met.* **56** 2670 (1993)
102. C Letouze, C Bonfait, C Shlenker, J Dumas, M Almeida, M Greenblatt, Z S Teweldemedhin *J. Phys. I* **5** 437 (1995)
103. C Hess, C LeTouze, C Schlenker, J Dumas, D Groult *Synt. Met.* **86** 2157 (1997)
104. N Witkowski, M Garnier, D Purdie, Y Baer, D Malterre, D Groult *Solid State Commun.* **103** 471 (1997)
105. C Hess, C Letouze, C Schlenker, J Dumas, D Groult, J Marcus *Synt. Met.* **86** 2419 (1997)
106. C Hess, A Ottolenghi, J P Pouget, C Shlenker, J L Hodeau, J Marcus *Synth. Met.* **86** 2169 (1997)
107. H Guyot, N Motta, J Marcus, S Drouard, B Balaska, in *Proceedings of the 19th European Conference on Surface Science (ECOSS-19), Madrid, 2000* Vol. 1, p. 54
108. E Canadell, M-H Whangbo *Int. J. Mod. Phys. B* **7** 4005 (1993)
109. E Canadell, M-H Whangbo *J. Solid State Chem.* **86** 131 (1990)
110. C M Varma, P B Littlewood, S Schmitt-Rink *Phys. Rev. Lett.* **63** 1996 (1989)
111. Y F Yan, M Kleman, C LeTouze, J Marcus, C Schlenker, in *Extended Abstract of the 13th International Conference on Electronic Microscopy* (Eds B Jouffrey, C Collieux) (Paris: Les Editions de Physique, 1994) Vol. IIB, p. 909
112. Y Yan, M Kleman, C Letouze, J Marcus, C Schlenker, A Buffat *Europhys. Lett.* **30** 49 (1995)
113. E Sandre, P Foury-Leylekian, S Ravy, J-P Pouget *Phys. Rev. Lett.* **86** 5100 (2001)
114. O Perez, P Roussel, H Guyot *Tech. Rep. Institut Max von Laue – Paul Langevin (Grenoble)* **1** 23 (2000)
115. X W Lou, H C Zeng *Inorg. Chem.* **42** 6169 (2003)
116. G R Patzke, F Krumeich, R Nesper *Angew. Chem., Int. Ed.* **41** 2446 (2002)
117. Y Xia, P Yang, Y Sun, Y Wu, B Mayers, B Gates, Y Yin, F Kim, H Yan *Adv. Mater.* **15** 353 (2003)
118. C N R Rao, A K Cheetham *J. Mater. Chem.* **11** 2887 (2001)
119. C N R Rao, G U Kulkami, P J Thomas, P P Edwards *Chem. Eur. J.* **8** 29 (2002)
120. N I Kovtyukhova, T E Mallouk *Chem. Eur. J.* **8** 4354 (2002)
121. C G Granqvist *Sol. Energy Mater. Sol. Cells* **60** 201 (2000)
122. I Turyan, U Q Krasovec, B Orel, T Saraidorov, R Reisfeld, D Mandler *Adv. Mater.* **12** 330 (2000)
123. W M Qu, W Wlodarski *Sens. Actuators, B,* **64** 42 (2000)
124. X Z Li, F B Li, C L Yang, W K Ge *J. Photochem. Photobiol., A* **141** 209 (2001)
125. C Santato, M Odziemkowski, M Ulmann, J Augustynski *J. Am. Chem. Soc.* **123** 10 639 (2001)
126. T Millner, J Neugebauer *Nature (London)* **163** 601 (1949)
127. J Pfeifer, E Badaljan, P Tekula-Buxbaum, T Kovacs, O Geszti, A L Toth, H-J Lunk *J. Cryst. Growth* **169** 727 (1996)
128. H Qi, C Wang, J Liu *Adv. Mater.* **15** 411(2003)
129. Y B Li, Y Bando, D Golberg, K Kurashima *Chem. Phys. Lett.* **367** 214 (2003)
130. Z Liu, Y Bando, C Tang *Chem. Phys. Lett.* **372** 179 (2003)
131. V K Yatsimirsky, V V Lisnyak, N V Stus, N S Slobodyanik, in *Proceedings of the 5th European Congress of Catalysis, Limerick, 2001* p. 37
132. V V Lisnyak, N S Slobodyanik, V K Yatsimirsky, N A Boldyreva, in *Studies in Surface Science and Catalysis* Vol. 130 (Eds A Corma, F V Melo, S Mendioroz, J L G Fierro) (Amsterdam, London, New York, Paris, Geneva, Bern, Tokyo, Seoul, Sydney: Elsevier, 2000) p. 3807

133. V V Lisnyak, N S Slobodyanik, V K Yatsimirsky, in *Proceedings of the 4th European Congress of Catalysis, International Conference on CO Catalyst, Remini, 1999* p. 837
134. T L Adelman, S V Zaitsev-Zotov, R E Thorne *Phys. Rev. Lett.* **74** 5264 (1995)
135. H S J van der Zant, O C Mantel, C Dekker, J E Mooij, C Traeholt *Appl. Phys. Lett.* **68** 3823 (1996)
136. V V Lisnyak, N V Stus, M S Slobodyanik, in *Proceedings of International Conference Functionalized Materials: Synthesis, Properties and Application, Kyiv, 2002* p. 55
137. V V Lisnyak, N V Stus, M S Slobodyanik, in *Proceedings of International Conference Functionalized Materials: Synthesis, Properties and Application, Kyiv, 2002* p. 144
138. V V Lisnyak, N V Stus, V S Sudavtzova, P Popovich, N S Slobodyanik, in *Science for Materials in the Frontier of Centuries Advantages and Challenges* Vol. 2. (Ed. V Skorohod) (Kyiv: European Material Research Society, National Academy of Science of Ukraine, Frantsevich Institute for Problem of Material Science, 2002) p. 233